The microbiome shapes immunity in a sex-specific manner in mouse models of Alzheimer's disease

John W. Bostick[1,*], Trista J. Connerly[1,2], Taren Thron[1], Brittany D. Needham[1,2,3], Matheus de Castro Fonseca[1], Rima Kaddurah-Daouk[4,5,6], Rob Knight[7], and Sarkis K. Mazmanian[1,*]

[1] Division of Biology and Biological Engineering, California Institute of Technology, Pasadena, California, USA.
[2] Present address: Stark Neurosciences Research Institute, Indiana University School of Medicine, Indianapolis, Indiana, USA.
[3] Present address: Department of Anatomy, Cell Biology & Physiology, Indiana University School of Medicine, Indianapolis, Indiana, USA.
[4] Department of Psychiatry and Behavioral Sciences, Duke University, Durham, North Carolina, USA.
[5] Duke Institute of Brain Sciences, Duke University, Durham, North Carolina, USA.
[6] Department of Medicine, Duke University, Durham, North Carolina, USA.
[7] Department of Pediatrics, Shu Chien-Gene Lay Department of Bioengineering, Computer Science & Engineering and Halicioğlu Data Science Institute, University of California San Diego, La Jolla CA USA.

*Correspondence: John W. Bostick, john.w.bostick@gmail.com; Sarkis K. Mazmanian, sarkis@caltech.edu

Abstract
INTRODUCTION: Preclinical studies reveal that the microbiome broadly affects immune responses and the deposition and/or clearance of amyloid-beta (Aβ) in mouse models of Alzheimer's disease (AD). Whether the microbiome shapes central and peripheral immune profiles in AD models remains unknown.
METHODS: We examined adaptive immune responses in two mouse models containing AD-related genetic predispositions (3xTg and 5xFAD) in the presence or absence of the microbiome.
RESULTS: T and B cells were altered in brain-associated and systemic immune tissues between genetic models and wildtype mice, with earlier signs if inflammation in female mice. Systemic immune responses were modulated by the microbiome and differed by sex. Further, the absence of a microbiome in germ-free mice resulted in reduced cognitive deficits, primarily in female mice.
DISCUSSION: These data reveal sexual dimorphism in early signs of inflammation and the effects of the microbiome, and highlight a previously unrecognized interaction between sex and the microbiome in mouse models of AD.

Keywords
Alzheimer's disease, animal models, 3xTg, 5xFAD, mice, microbiome, germ-free, adaptive immunity, inflammation, sex-specific

Research in Context

1. **Systemic review**: We reviewed the literature related to Alzheimer's disease (AD), inflammation, and the microbiome using PubMed. We cite several studies that demonstrate the influence of the microbiome on inflammation and cognitive performance in both animal models and humans. However, the mechanisms linking immunity to AD are not well understood.

2. **Interpretation**: Using two well-established mouse models of AD, we found that the microbiome does not strongly influence the onset of inflammation in brain-draining lymph nodes; rather, it largely modulates systemic immune responses, local cytokine production, and cognitive performance. Notably, the inflammatory state in mice was affected by sex, and this sex effect differed between local and systemic tissues and mice with or without a microbiome.

3. **Future directions**: Our work identified a sex- and microbiome-mediated effect on inflammation and cognitive performance. Future studies may focus on microbiome-dependent mechanisms that intersect with sex hormone and immune responses to determine peripheral effects on AD outcomes.

Highlights

- Adaptive immunity is activated at early ages and differentially by sex in mouse models of AD.
- Inflammation in 5xFAD mice is characterized by increased IL-17A-producing T cells.
- Inflammation in 3xTg mice is characterized by increased cytokine responses in males, but attenuated cytokine responses in female mice.
- Longitudinal immune responses differ between 3xTg mice and 5xFAD mice.
- Both 3xTg and 5xFAD female mice show improved learning and cognition in the absence of a microbiome.

1 BACKGROUND

Alzheimer's disease (AD) is the most prevalent neurodegenerative disease, and its incidence is expected to increase further as the global population ages [1]. Considerable progress has been made in understanding cellular and molecular contributors to AD; however, much remains unknown about its development and pathological mechanisms. Approximately two-thirds of AD cases in the United States are in females, prompting the question of how sex influences susceptibility [1]. Although many people accumulate amyloid-β (Aβ) plaques, a key pathological hallmark of AD, only a subset will develop AD. Genetics cannot completely explain the differences [1,2]. Recent research has implicated lifestyle and environmental factors, including diet and the microbiome: the collection of microorganisms that colonize the human body [3–8]. Animal models, such as transgenic rodents, provide an opportunity to explore these questions.

AD is characterized by the accumulation of Aβ plaques and tau-mediated neurofibrillary tangles, leading to neuroinflammation, impaired synaptic communication, neuronal death, and decline in cognitive function. Two widely used models of AD are the 3x transgenic (3xTg) and 5x familial Alzheimer's disease (5xFAD) mouse models [9,10]. These preclinical models employ overexpression of genes with known AD association to translate human pathophysiology into mice. Both models develop AD-associated Aβ aggregates, and the time course of disease is characterized, which motivates their use in this study. Due to expression of the tau protein in the 3xTg model, tau fibrils accumulate at 12 months, but not in the 5xFAD model [11]. While the immune response in the central nervous system (CNS) of both animal models has been extensively characterized, less is known about immune responses in peripheral tissues outside the CNS or the effect of the microbiome on immunity.

Prior evidence from AD models has revealed inflammation associated with Aβ and tau accumulation in the CNS [12]. Inflammatory responses by astrocytes and microglia, two cell types that interact closely with neurons and promote their function, may contribute to initial innate immune responses [13]. These cells are important components of protective Aβ clearance pathways. The adaptive immune response is directed at specific molecular targets that activate T and B cell receptors in an antigen-specific manner. As pathology progresses, the adaptive immune system is activated, although the initiating events, molecular targets, and timing are not

well understood. Nonetheless, T and B cell responses can be protective in AD animal models, as genetic depletion of these cells results in greater accumulation of plaques and increased cytokine production [14]. Paradoxically, eliminating B cells alone is protective against AD-like progression in mice, indicating a B cell contribution to pathogenic processes [15]. Thus, there remains a need to resolve the protective and pathogenic mechanisms of T and B cell contributions to AD and its relevant mouse models.

The intestinal microbiome influences outcomes related to AD [7,16]. In AD mouse models, germ-free (GF) conditions or antibiotic treatment reduces Aβ aggregates in the brain [3–5]. In addition, the microbiome regulates inflammatory responses in AD [6,7]. Microbes and microbe-produced factors may affect AD in several ways, but one important aspect is activating immune cells [17,18]. However, understanding the mechanisms by which the microbiome exerts these influences on AD requires further investigation.

Herein, we investigated immune responses in mice with AD-associated genetic landscapes in the presence or absence of the microbiome by comparing germ-free (GF) to conventionally raised specific pathogen free (SPF) mice, i.e., those with the normal laboratory microbiota, with the same genotype. We found that adaptive immune responses were elevated in multiple tissues and varied by sex and microbiome status. Specifically, we show that the time of onset of the adaptive immune response in brain-draining lymph nodes is sex-dependent, occurring earlier in female mice. In the 3xTg model, immune responses were dramatically elevated when males, but not females, were kept germ-free. In contrast, the 5xFAD model showed increased signs of inflammation in females compared to males in SPF conditions. Importantly, the absence of a microbiome attenuated immune responses and improved cognitive function, primarily in female mice in both models. Our results demonstrate that the microbiome and sex interact to influence immunity and cognition in mouse models of AD.

2 METHODS

2. 1 Mice

Wildtype C57BL/6J (The Jackson Laboratory, Cat#000664) mice were obtained from Jackson Laboratory at 8 weeks of age. Homozygous 3xTg [B6;129-Tg(APPSwe,tauP301L)1LfaPsen1TM1 Mpm/Mmjax] and Hemizygous 5xFAD [B6.Cg-Tg(APPSwFlLon,PSEN1*M146L*L286V)6799Vas/Mmjax] (The Jackson Laboratory, Cat#004807 and Cat#034848) mice were obtained from a colony maintained in the laboratory of S.K.M at the California Institute of Technology (Caltech). 5xFAD hemizygous mice and wildtype littermates were produced by crossing transgenic with C57BL/6J mice. C57BL/6J, 3xTg, and 5xFAD mice were rederived as germ-free (GF) in the Caltech gnotobiotic facility. After weaning, mice were housed together with littermates and aged until the experiment dates. All experiments were performed with female and male mice. For behavioral experiments, investigators were not blinded to group unless otherwise specified.

Experimental mice were housed in sterilized microisolator cages and maintained on ad libitum autoclaved 5010 PicoLab Rodent Diet (LabDiet, Cat#5010) and sterilized water. Germ-free mice were maintained on antibiotics water during behavioral tests [ampicillin (1mg/mL); vancomycin (0.5mg/mL); neomycin (1mg/mL)]. Animals were group housed (2–5 mice per cage) unless otherwise specified. Ambient temperature in the animal housing facilities was maintained at 21-24°C, 30-70% humidity, with a cycle of 13 hours light, 11 hours dark. All experiments were performed with approval from the Institutional Animal Care and Use Committee (IACUC) of Caltech (Protocol IA20-1798).

2.2 Immune cell isolation and profiling

2.2.1 Intestinal lamina propria immune cell isolation

For isolation of intestinal lamina propria cells, the small and large intestines were dissected and placed immediately into ice-cold phosphate-buffered solution (PBS). After mesenteric fat and Peyer's patches (small intestine) were removed, the intestines were longitudinally opened, and luminal contents were washed out with cold PBS. Tissue pieces were washed for 10 min. in 1 mM dithiothreitol (DTT)/PBS at room temperature on a rocker to remove mucus, followed by a wash for 25 min. in 10 mM EDTA/30 mM HEPES/PBS at 37 °C on a platform shaker (180 rpm)

to remove epithelium. After a 2 min. wash in complete RPMI, the tissue was digested in a six-well plate for 1.5 hr. in complete RPMI with 150 U/mL (small intestine) or 300 U/mL (large intestine) collagenase VIII (Sigma-Aldrich) and 150 µg/mL DNase (Sigma-Aldrich) in a cell culture incubator (5% CO_2). Tissue digests were passed through a 100 µm cell strainer and separated by centrifugation (1250g for 20 min.) using a 40/80% Percoll gradient. Immune cells were collected at the 40/80% interface and washed with HBSS wash buffer [1xHBSS without phenol red, Ca^{2+}, or Mg^{2+}; 10mM HEPES buffer, DNAse1 (50ug/ml), 1mM MgCl2, and BSA Fraction V (2.5mg/ml)] before surface staining, fixation (eBioscience Foxp3 / Transcription Factor Staining Buffer Set), and intracellular staining.

2.2.2 Spleen and lymph node immune cell isolation

For the spleen and lymph nodes, the tissue was passed through a 100 µm cell strainer and washed with HBSS wash buffer. The spleen suspension was centrifuged at 500g for 5 min., resuspend in red cell lysis buffer (Sigma-Aldrich), and incubated for 8 min. at room temperature. Spleen and lymph node cell suspensions were washed with 0.5% BSA/PBS before surface staining and fixation (eBioscience Foxp3 / Transcription Factor Staining Buffer Set).

2.2.3 Immune cell profiling by flow cytometry

For flow cytometry staining, CD16/32 antibody (eBioscience) was used to block non-specific binding to Fc receptors before surface staining at 4C for 30 min. Immune cells were stained with antibodies against the following markers: CD19 (FITC), CD3e (PE), CD4 (APC; BV510), CD45.2 (BV421), CD8a (APC-e780), Foxp3 (APC), IFNγ (FITC), IL-17A (PE), and TCRβ (PerCP-Cy5.5). Live and dead cells were discriminated by Live/Dead Fixable Violet or Aqua Dead Cell Stain Kit (Invitrogen).

2.3 Behavior Testing

Noldus Ethovision software (Wageningen, Netherlands) was used to record animal behavior and analyses were performed utilizing the Ethovision software.

2.3.1 Y Maze Protocol

Spatial memory was assessed by spontaneous alternation measurement in a three-arm open maze as described previously [19]. Mice were acclimated in the behavior room for thirty minutes prior to testing. Each arm was assigned a letter (A, B, or C). Mice were placed into Arm C and then allowed a period of five minutes to explore the maze. At the end of five minutes, the mouse was removed from the maze. The maze was thoroughly cleaned with a 0.5% hydrogen peroxide disinfectant and allowed to dry to remove olfactory cues. A camera mounted above the center of the maze was utilized to identify the center point of each mouse. Arm entries and re-entries were counted manually. An arm entry was counted if the center point of the mouse crossed the threshold between the arm and center. If a mouse entered an arm momentarily, returned to the center of the maze, and then entered the same arm again, this was considered as two entries to the same arm. Spontaneous alternations were classified as successive entries into three successive arms without error. Percent alternations was calculated with the following equation:
% alternations = (# spontaneous alternations/total number of arm entries -2) x 100

2.3.2 Novel Object Recognition

Mice were moved into the behavior room thirty minutes prior to assessment on day one to acclimate. Mice were assessed over two days and housed overnight in the behavior room between assessment days. Mice were placed into a box with two similar objects, either two 8” x 4” colored blocks, or two cell culture flasks filled with sand, and allowed to roam the box for ten minutes as described previously [20]. These first objects were referred to as the “familiar object.” Initial familiar objects were alternated between the colored blocks and flasks to avoid object bias. The following day, a “novel object” replaced one of the familiar objects and the mice were allowed to assess the field and objects for an additional ten minutes. Time spent at each object was recorded and documented by the Ethovision software. The following formula was used in description of the relation between the total time spent at the objects and the time spent at each object: Recognition Index = time spent investigating the novel object / (time spent investigating the familiar object + time spent investigating the novel object)

2.3.3 Barnes Maze

We followed the shortened Barnes Maze protocol outlined in Attar et al. [21]. The procedure included a habituation period, four training periods, and a final test period. All mice were habituated for a minimum of thirty minutes in the behavior room to allow for adjustment to their surroundings. We maintained a minimum of one hour between the habituation period and training periods. Each cohort completed a habituation period and two training periods on day one. Two more training sessions were completed on day two. Mice were rested on day three and tested on day four. The Barnes Maze has eighteen equally spaced holes around the perimeter of a circular maze. The goal box was always aligned in the same position relative to visual cues in the room. Four reference objects were used during all periods of testing to orientate the mice around the room, in addition to the natural asymmetry of the behavior room. In the habituation phase, mice were guided to a dark goal box located beneath the target hole. Aversive stimuli, including bright diffuse light, fan-induced air currents, and white noise provided encouragement for the mice to find the goal box during the trainings and test day. During each training, mice were allowed 180 seconds to locate and enter the goal box. When the mouse entered the goal box, the aversive noise machine was turned off via remote. Mice were allowed twenty seconds to further acclimate to the goal box before being returned to their home cage. If the mouse did not enter the goal box on their own within 180 seconds, they were guided to the goal box and allowed to acclimate for twenty seconds without the aversive noise. They were then returned to their home cage. On the test day, the goal box was removed, and the mice were allowed to roam for 120 seconds. We assessed the latency in seconds required for mice to escape over the trainings and on test day.

2.4 Statistical Methods

Unless otherwise noted, statistical analyses for behavior tests were performed with the non-parametric Mann-Whitney U test and two-way ANOVA for immune response data on individual biological samples with GraphPad Prism 10.0. Two-way ANOVA analyses were corrected for multiple comparisons. Unless otherwise noted, only statistical comparisons with $p<0.05$ are shown. *$p<0.05$, **$p<0.01$, ***$p<0.001$, ****$p<0.0001$, n.s. not significant.

3 RESULTS

3.1 Adaptive immunity is enhanced in early life and differentially by sex in mouse models of AD.

To evaluate the contribution of the microbiome to inflammation in Alzheimer's disease (AD), we examined immune responses in two well-established mouse models (3xTg and 5xFAD) [9,10] in the presence or absence of the microbiome, utilizing specific pathogen free (SPF; i.e., laboratory microbiota) and germ-free (GF) mice (**Figure S1**). We analyzed both local (tissue-specific draining lymph nodes) and systemic (spleen) immune responses in male and female mice at ages corresponding to previously reported onset and progression of AD-related pathology: 7, 12, and 15 months for the 3xTg model and 5 and 8 months for the 5xFAD model.

In the superficial and deep cervical lymph nodes (CLNs), which are the primary draining lymph nodes for the lymphatics associated with the brain, head, and neck, we found that $CD4^+$ T cell frequencies and numbers in the cervical lymph nodes were elevated in female 3xTg mice at the earliest age measured (7 months), whether the mice were raised under GF or SPF conditions (**Figure 1A and B**; **Figure S2A and B**). This indicates an activated adaptive immune response in brain-associated lymph nodes, before the onset of behavioral deficits at 12 months of age, as previously reported [22,23]. T cell increases in the CLNs were driven by $CD4^+$ (helper) T cells, (**Figure 1A and 1B**) as well as $CD8^+$ (cytotoxic) T cells in the deep CLNs (**Figure S2D**). Notably, there were no significant increases in $CD4^+$ T cell frequencies in male 3xTg mice at the same age, indicating sexual dimorphism in immune responses in the 3xTg model at this early age (**Figure 1A and B; Figure S2A-D**). This parallels previously described differences in the onset of Aβ plaque accumulation in the brains of 3xTg mice [11,22,24], with female mice showing plaques in the hippocampus and cortex and impaired cognitive function at ages earlier than males [11,25]. We found decreased B cell numbers in the superficial CLNs of GF and SPF female 3xTg mice (**Figure S3A**), indicating differential rates of accumulation or egress between T and B cells in the lymph node. No changes were observed in the deep CLNs (**Figure S3B**).

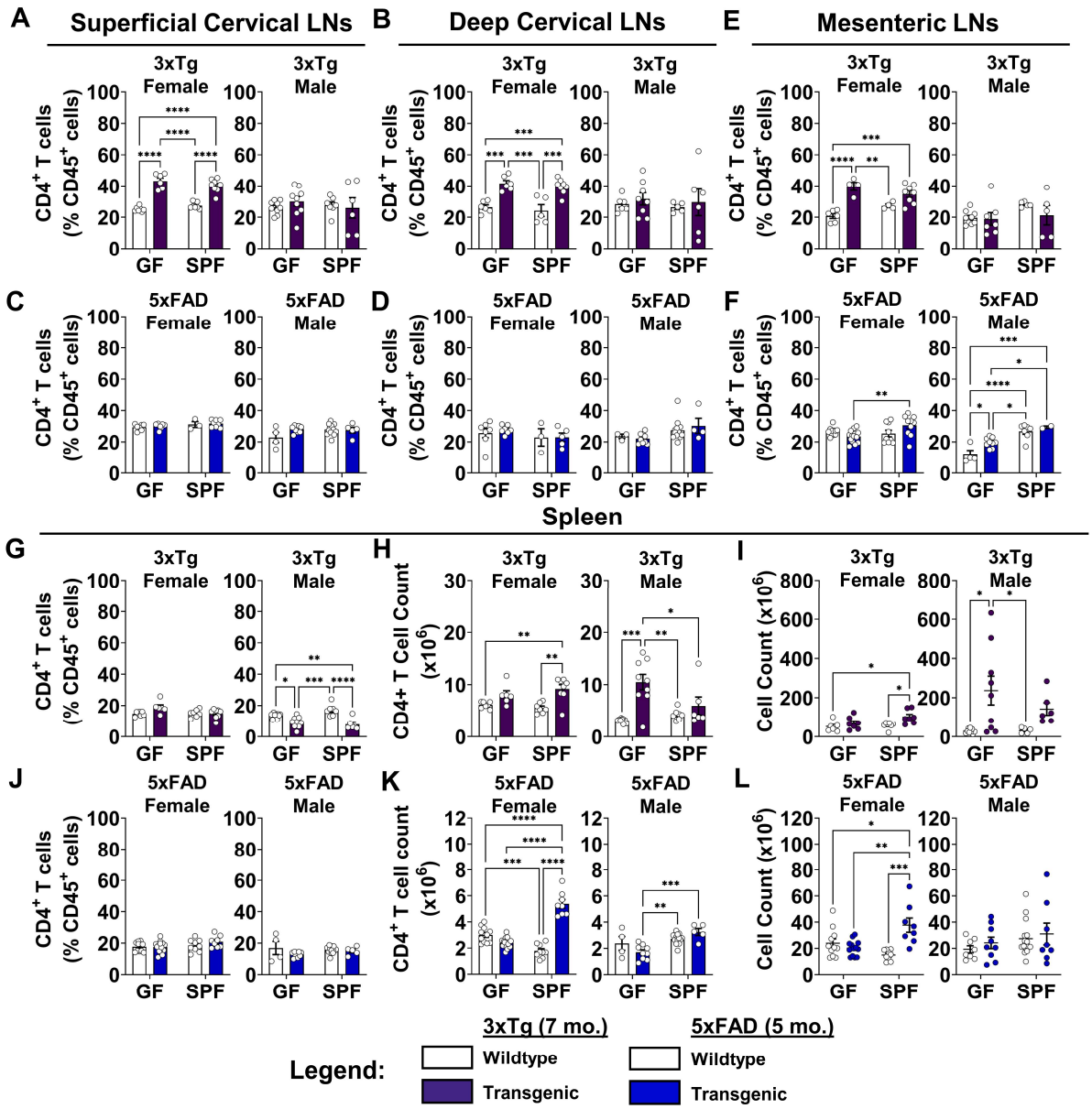

Figure 1. Adaptive immunity is activated early and differentially by sex in mouse models of AD
(A) Quantification of CD4$^+$ T cell frequencies in the superficial cervical lymph nodes of female (Left) and male (Right) 3xTg mice compared to wildtype controls in germ-free (GF) and specific pathogen free (SPF) conditions at 7 months of age. (B) Deep cervical lymph nodes. Data are pooled from 2 independent experiments (n = 4 to 8 per group); two-way ANOVA. (C) Superficial cervical lymph nodes of female (Left) and male (Right) 5xFAD mice at 5 months of age. (D) Deep cervical lymph nodes. Data are pooled from 2 independent experiments (n = 4 to 10 per group); two-way ANOVA. (E) Mesenteric lymph nodes of female (Left) and male (Right) 3xTg and (F) 5xFAD mice. Data are pooled from 2 independent experiments (n = 4 to 10 per group); two-way ANOVA. (G) Spleens of female (Left) and male (Right) 3xTg mice. (H) Quantification of 3xTg spleen CD4$^+$ T cell counts. (I) Cell counts in the spleens of female (Left) and male (Right) 3xTg mice. Data are pooled from 2 independent experiments (n = 6 to 9 per group); two-way ANOVA. (J) Quantification of CD4$^+$ T cell frequencies in the spleens of female (Left) and male (Right) 5xFAD mice. (K) Quantification of 5xFAD spleen CD4$^+$ T cell counts. (L) Cell counts in the spleens of female (Left) and male (Right) 5xFAD mice. Data are pooled from 2 independent experiments (n = 4 to 12 per group); two-way ANOVA. Error bars indicate SEM. *P < 0.05, **P < 0.01, ***P < 0.001, ****P < 0.0001; ns, not significant.

In contrast in the 5xFAD mouse model, we observed no changes in $CD4^+$ T cell frequency in the CLNs in female or male mice at the earliest age measured (5 months) (**Figure 1C and D**). However, decreases in total T cell numbers (**Figure S2E and F**) and B cell numbers (**Figure S3E and F**) were observed in the CLNs, though not all comparisons followed this pattern.
In the mesenteric lymph nodes (MLNs), which drain the small and large intestines, we observed elevated T and B cell numbers in both SPF female and male 3xTg mice at 7 months of age, but not in GF mice, indicating adaptive immunity-mediated inflammation in the intestines that is microbiome dependent (**Figure S2G and S3C**). However, $CD4^+$ T cell proportions in the MLNs increased in both GF and SPF female mice (**Figure 1E**). $CD8^+$ T cell numbers in the MLNs were unaffected by genotype and microbiome status (**Figure S2H**).

In female 5xFAD mice at 5 months, there was no significant difference in $CD4^+$ T cell frequencies from wildtype (WT) mice, but a slight increase was observed between GF and SPF conditions (**Figure 1F**). However, SPF male 5xFAD mice displayed an increase in $CD4^+$ T cell frequencies regardless of genotype (**Figure 1F**). B cell numbers were elevated in female 5xFAD mice under GF conditions, while SPF mice paradoxically showed lower B cell counts (**Figure S3G**).

We next assessed systemic inflammation by examining immune responses in the spleen. $CD4^+$ T cell frequencies were decreased in male, but not female, 3xTg mice under both housing conditions (**Figure 1G**). However, total $CD4^+$ T cell numbers were elevated in both female and male 3xTg mice, with the greatest increase in GF male mice (**Figure 1H**). These increased $CD4^+$ T cell numbers tracked with an increased overall number of cells in the spleen (splenomegaly), consistent with previous observations of splenomegaly in this model (**Figure 1I**) [26,27]. In female 3xTg mice, spleen size, quantified by cell counts, doubled in SPF conditions (**Figure 1I**). In male mice, spleen cell counts increased more remarkably by 8- and 4-fold in GF and SPF conditions, respectively (**Figure 1I**). The greater increase in spleen cellularity in GF male mice was unexpected and suggests a sex-dependent role for the microbiome in systemic inflammation in 3xTg mice. 5xFAD mice showed no changes in $CD4^+$ T cell frequencies and slight increases in B cell frequencies (**Figure 1J and S2I**), but again, significant increases in total $CD4^+$ T cell and B cell numbers were observed, an effect which was more pronounced in SPF female mice

(**Figure 1K and L; Figure S3H**), consistent with previous suggestions of autoimmune-like inflammation in both models [26,28,29].

Together, these results show elevated adaptive immune responses both in locally draining lymph nodes (brain and intestine) and systemically (spleen) at the earliest ages examined in both models. In 3xTg mice, $CD4^+$ T cell numbers in CLNs were elevated in female mice, but not male mice, regardless of microbiome status. Systemic immune responses were modulated by the microbiome and differed by sex, with increased immune cell numbers in GF males. In 5xFAD mice, increases in T and B cell numbers were restricted to the spleen and MLNs, suggesting less pronounced immune responses than in 3xTg mice. These data reveal sexual dimorphism in both inflammation onset and the effects of the microbiome in these mouse models. It is not clear whether the elevated $CD4^+$ T cells and B cells participate in protective or pathogenic roles.

3.2 Inflammation in 3xTg mice is characterized by increased cytokine responses in males, but attenuated cytokine responses in females.

To characterize the quality of T cell responses, we examined cytokine production and profiled effector and regulatory T cells in both the 3xTg and 5xFAD models. The cytokine, interleukin (IL)-17A, has been implicated in the pathogenesis of neurodegenerative diseases including stroke, multiple sclerosis, AD, and Parkinson's disease [30]. IL-17A is expressed at barrier and mucosal surfaces, including the skin, gastrointestinal and urogenital tracts, and is induced by specific bacterial taxa of the microbiome that colonize environmentally exposed surfaces of the body [30,31]. The functional role of IL-17A in the CNS is under active investigation, but data suggests that this cytokine promotes neuroinflammation [25,30,32,33]. In 12-month-old male

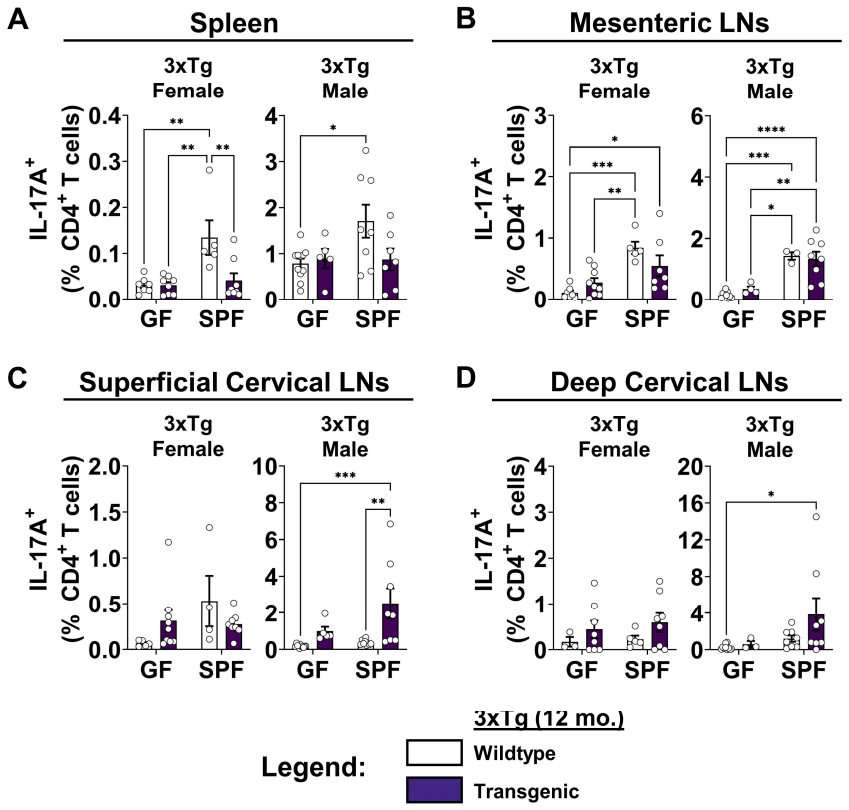

Figure 2. Inflammation in 3xTg mice is characterized by increased cytokine responses in males, but attenuated cytokine responses in females.
(A) Quantification of IL-17A$^+$ T cell frequencies in the spleens of female (Left) and male (Right) 3xTg mice compared to wildtype controls in germ-free (GF) and specific pathogen free (SPF) conditions at 12 months of age. (B) Mesenteric lymph nodes. (C) Superficial cervical lymph nodes. (D) Deep cervical lymph nodes. Data are pooled from 2 independent experiments (n = 3 to 10 per group); two-way ANOVA. Error bars indicate SEM. *P < 0.05, **P < 0.01, ***P < 0.001, ****P < 0.0001; ns, not significant.

3xTg mice, we observed elevated IL-17A$^+$ CD4$^+$ T cells in the superficial and deep CLNs (**Figure 2A-D**), despite unchanged overall CD4$^+$ T cell frequencies (**Figure S4A-D**). There were minimal changes in either the spleen or MLNs in SPF male 3xTg mice for IL-17A. Increased IL-17A$^+$ CD4$^+$ T cells were more pronounced in SPF mice compared to the GF counterparts. In contrast, female 3xTg mice did not have statistically significant increases in the frequencies of cytokine-producing T cells (**Figure 2A-D**), despite showing elevated CD4$^+$ T cell frequencies (**Figure S4A-D)**. Together, these data indicate that T cell proportions are elevated in 3xTg female mice, but cell activation is attenuated, whereas the opposite effect occurs in males.

In inflamed environments, regulatory T cell numbers increase with expanding cytokine-producing effector T cells and act to limit immune responses [34,35]. A major subset of CD4$^+$ regulatory T cell is marked by the forkhead box transcription factor P3 (Foxp3). Foxp3$^+$ T cell frequencies were not significantly changed between transgenic and WT mice but were reduced in SPF mice compared to GF mice in most tissues and both sexes (**Figure S5A-D**). Reduced

regulatory T cell frequencies in 3xTg mice are therefore consistent with the increased inflammation that we observed in this mouse model.

3.3 Inflammation in 5xFAD mice is characterized by increased IL-17A-producing T cells.

Consistent with the role of the microbiome in promoting IL-17A production [30,31], we found that IL-17A$^+$ T cells in the intestines of 5xFAD mice are increased by the presence of the microbiome (i.e., SPF conditions) (**Figure 3A and B**).

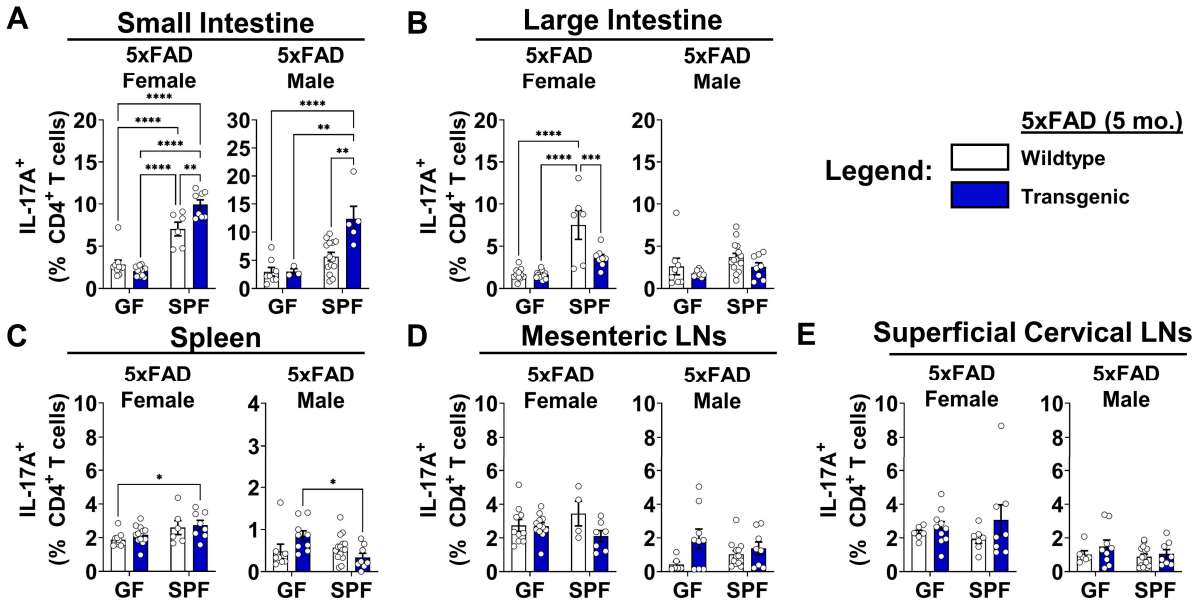

Figure 3. Inflammation in 5xFAD mice is characterized by increased IL-17A-producing T cells. (A) Quantification of IL-17A$^+$ T cell frequencies in the small intestines of female (Left) and male (Right) 5xFAD mice compared to wildtype controls in germ-free (GF) and specific pathogen free (SPF) conditions at 5 months of age. (B) Large intestine. (C) Spleen. (D) Mesenteric lymph nodes. (E) Superficial cervical lymph nodes. Data are pooled from 2 independent experiments (n = 4 to 14 per group); two-way ANOVA. Error bars indicate SEM. *P < 0.05, **P < 0.01, ***P < 0.001, ****P < 0.0001; ns, not significant.

Importantly, and unexpectedly, we found IL-17A-producing CD4$^+$ T cells were further increased in the small intestines of SPF 5xFAD transgenic female and male mice compared to wildtype controls at 5 months age (**Figure 3A**). Previous reports indicated reduced IL-17A production in the gut-associated immune populations of 5xFAD transgenic mice, specifically in the mesenteric lymph nodes and Peyer's patches [36]. Indeed, we observed lower IL-17A$^+$ T cell frequencies in the large intestine, spleen, and MLNs of SPF transgenic mice (**Figure 3B-D**). We found no changes in IL-17A$^+$ T cell frequencies or counts in the superficial CLNs (**Figure 3E and S6A**). The increase in the IL-17A$^+$ T cell populations in the small intestine tissue (lamina propria)

(**Figure 3A**) vs. the large intestine and MLNs (**Figure 2B and D**) indicates the environment of the small intestine was specifically conducive to either IL-17A$^+$ T cell differentiation, proliferation, and/or cell retention. In accordance with the observed splenomegaly (see **Figure 1L**), the total number of IL-17A$^+$ T cells dramatically increased in the spleens of SPF female 5xFAD mice (**Figure S6B**). We observed a moderate increase in IL-17A$^+$ T cell numbers in the MLN of GF male transgenic mice (**Figure S6C**). IL-17A$^+$ T cells play a significant role in autoimmunity [32,37]. The observed increase of IL-17A$^+$ T cells in the 5xFAD transgenic mice suggests increased autoimmune-like inflammation that is modulated by gut bacteria [35,36], an alteration in microbiome localization or composition in the intestines, or both.

We observed increased Foxp3$^+$ regulatory T cell frequencies and counts in the spleens, MLNs and deep CLNs of SPF female, but not male, 5xFAD mice (**Figure S7A, B, D and F**). Male mice showed lower proportions of Foxp3$^+$ T cells in the MLNs, superficial and deep CLNs, and large intestines, regardless of microbiome status (**Figure S7B, C, D and E**). Together, these data indicate increased inflammation that is balanced by the induction of regulatory T cells in female 5xFAD mice and decreased anti-inflammatory T cell populations in most tissues of SPF male 5xFAD mice. Whether this balance is maintained over increasing age and pathology development requires further examination.

3.4 Longitudinal immune responses differ between 3xTg mice and 5xFAD mice.

The most significant risk factor for AD is aging [1]. To determine how inflammation progressively changes in mouse models, we examined immune responses at multiple ages. In 3xTg mice, CD4$^+$ T cell counts that we observed at 7 months of age remained elevated in the spleens and MLNs of SPF female animals but declined by half in the CLNs from 7 to 15 months of age (**Figure 4A-D)**.

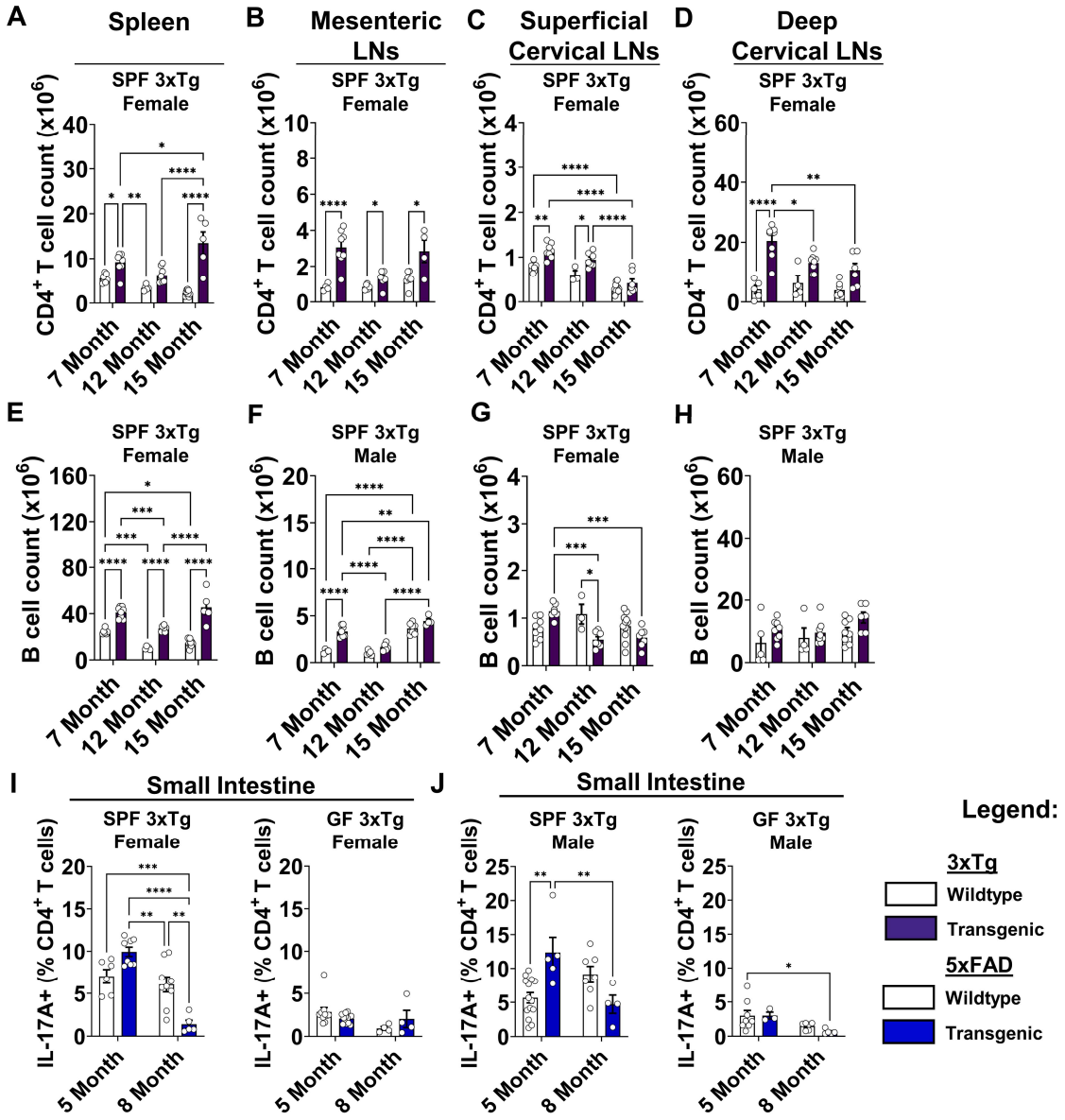

Figure 4. Longitudinal immune responses differ between 3xTg mice and 5xFAD mice.
(A) Quantification of $CD4^+$ T cell counts in the spleens of female 3xTg mice compared to wildtype controls in specific pathogen free (SPF) conditions at 7-, 12-, and 15-months age. (B) Mesenteric lymph nodes. (C) Superficial cervical lymph nodes. (D) Deep cervical lymph nodes. Data are pooled from 5 independent experiments (n = 3 to 8 per group); two-way ANOVA. (E) Quantification of B cell counts in the spleens of female 3xTg mice. (F) Mesenteric lymph nodes. (G) Superficial cervical lymph nodes. (H) Deep cervical lymph nodes. Data are pooled from 5 independent experiments (n = 3 to 11 per group); two-way ANOVA. For clarity, only significant comparisons of the same mouse group between ages or between transgenic and control mice at the same age are shown. (I) Quantification of IL-$17A^+$ T cell frequencies in the small intestines of female 5xFAD mice compared to wildtype controls in germ-free (GF) (Right) and specific pathogen free (SPF) (Left) conditions at 5- and 8-months age. (J) Small intestines of male 5xFAD mice. Data are pooled from 5 independent experiments (n = 4 to 14 per group); two-way ANOVA. Error bars indicate SEM. *P < 0.05, **P < 0.01, ***P < 0.001, ****P < 0.0001; ns, not significant.

$CD4^+$ T cell numbers remained the same or declined in GF female mice (**Figure S8A-D**). Both GF and SPF male mice showed progressive increases in $CD4^+$ T cells, only in the spleen, with minimal change in other tissues as animals aged (**Figure S8E-L**). B cell numbers mirrored $CD4^+$ T cell numbers in female (**Figure 4E-H, S9A-D**) and male (**S9E-L**) 3xTg mice.

In 5xFAD mice, by contrast to 3xTg animals, IL-$17A^+$ T cells were attenuated in the small intestine from 5 to 8 months in both female and male mice (**Figure 4I and J**). However, B cell numbers remained elevated in the spleens of SPF female, but not SPF male, mice from 5 to 8 months of age, indicating sustained systemic inflammation (**Figure S10A**). In the MLNs and CLNs, B cell numbers largely remained the same under GF conditions with some variability (**Figure S10D, F, and H**), and GF male mice showed a decline in B cell counts with age in the MLNs (**Figure S10D**). We found an age-dependent increase in B cells that was independent of disease in the superficial and deep CLNs of SPF female mice (**Figure S10E and G**). The differences between 3xTg and 5xFAD mice in immune responses as animals age, especially in GF conditions, suggest differing mechanisms of immune activation and resolution. Overall, these data reveal that inflammation develops early in some models of AD, is largely microbiome-dependent, and can be durable or can resolve as animals age.

3.5 Both 3xTg and 5xFAD female mice show improved learning and cognition in the absence of a microbiome.

We next sought to determine whether differences in immune response correlate with cognitive outcomes. It has been previously reported that AD mouse models displayed reduced amyloid plaques and improved cognitive function under GF conditions or after antibiotic treatment, compared to mice with an intact microbiome [3–5]. However, reported behavioral outcomes in these two preclinical models has varied widely with regards to presence of a phenotype, age, behavioral paradigm tested, and examination of the gut microbiota [23,24]. To obtain a broad view of the cognitive performance in both models using multiple testing paradigms across aging, SPF and GF mice were evaluated via modified the Barnes maze, Y maze, and novel object recognition tests. Overall phenotypes were subtle, consistent with several previous studies [23,24,38]. However, we observed the most robust differences in cognitive function between transgenic and wildtype mice in the modified Barnes maze, with differences both during training

day learning and test day performance (**Figure 5**).

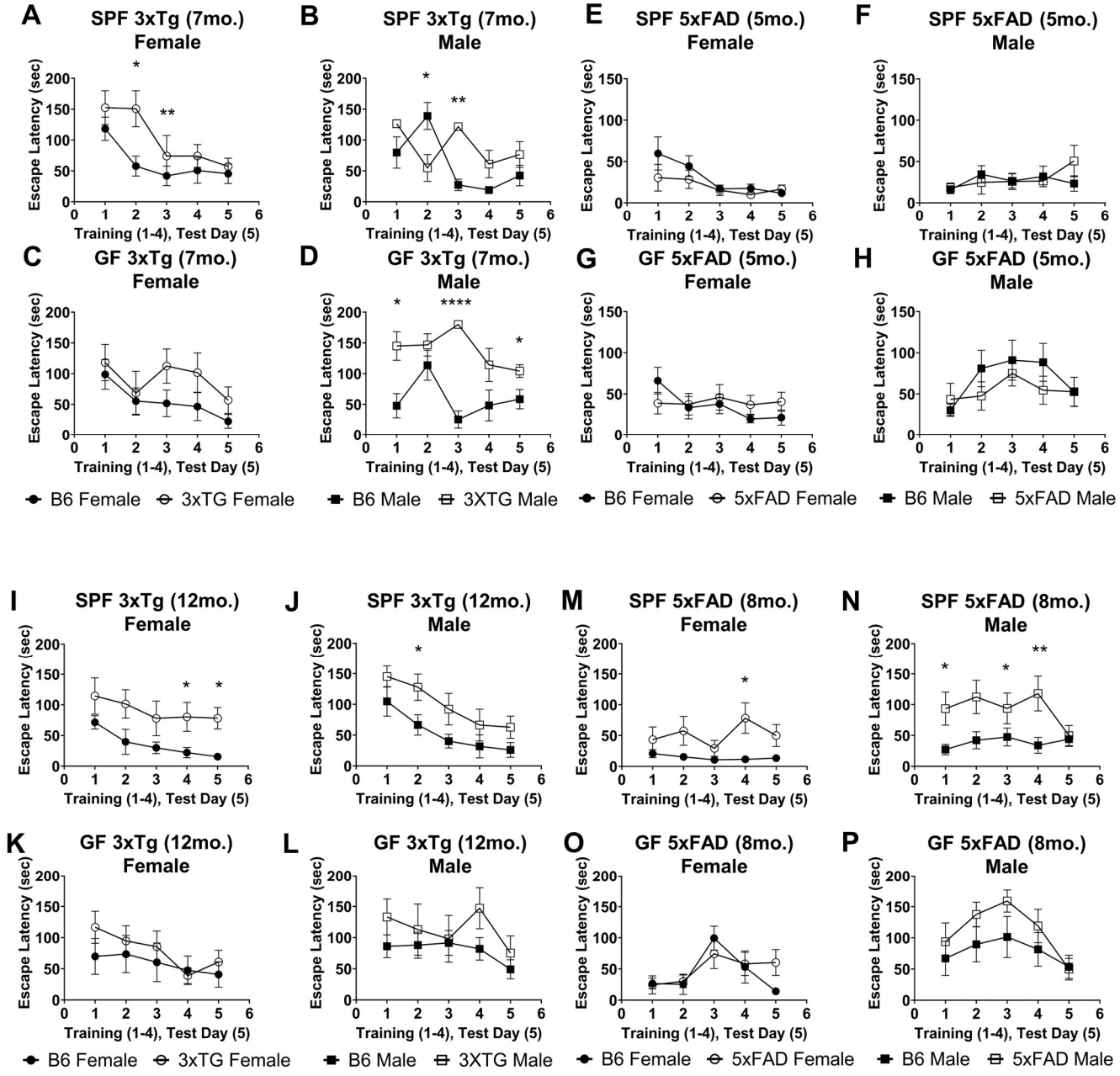

Figure 5. Both 3xTg and 5xFAD mice show improved learning and cognition in the absence of a microbiome.
(A) Training (1-4) and probe (5) day mean escape latency in Barnes Maze testing for cognitive deficits in 7-month-old female 3xTg mice compared to wildtype controls in specific pathogen free (SPF) conditions. (B) Male mice in SPF conditions. (C) Female mice in germ free (GF) conditions. (D) Male mice in GF conditions. Data are pooled from 2 independent experiments (n = 6 to 11 per group); (*) indicates Mann-Whitney U test comparing transgenic to control mice. (E) Training (1-4) and probe (5) day mean escape latency in Barnes Maze testing for cognitive deficits in 5-month-old female 5xFAD mice compared to wildtype controls in SPF conditions. (F) Male mice in SPF conditions. (G) Female mice in GF conditions. (H) Male mice in GF conditions. Data are pooled from 2 independent experiments (n = 8 to 14 per group). (I) Training (1-4) and probe (5) day mean escape latency in Barnes Maze testing for cognitive deficits in 12-month-old female 3xTg mice compared to wildtype controls in specific pathogen free (SPF) conditions. (J) Male mice in SPF conditions. (K) Female mice in germ free (GF) conditions. (L) Male mice in GF conditions. Data are pooled from 2 independent experiments (n = 5 to 11 per group); (*) indicates Mann-Whitney U test comparing transgenic to control mice. (M) Training (1-4) and probe (5) day mean escape latency in Barnes Maze testing for cognitive deficits in 8-month-old female 5xFAD mice compared to wildtype controls in SPF conditions. (N) Male mice in SPF conditions. (O) Female mice in GF conditions. (P) Male mice in GF conditions. Data are pooled from 2 independent experiments (n = 5 to 13 per group); (*) indicates Mann-Whitney U test comparing transgenic to control mice. Error bars indicate SEM. *P < 0.05, **P < 0.01, ***P < 0.001, ****P < 0.0001; ns, not significant.

Cognitive deficits, as measured by increased latencies to escape the maze, were more apparent in SPF mice compared to their GF counterparts, implicating the microbiome in this behavioral outcome. We observed cognitive deficits in both sexes in SPF 3xTg mice at 7 and 12 months of age (**Figure 5A,B,I, and J**) and SPF 5xFAD mice at 8 months of age (**Figure 5M and N**). Female mice had improved performance under GF conditions (**Figure 5C,G,K, and O**), whereas 7-month-old GF 3xTg males (**Figure 5D**) maintained cognitive deficits. Spatial memory testing with the Y-maze test did not show significant cognitive decline in male or female 3xTg mice at 7 or 12 months of age in either GF or SPF conditions (**Figure S11A-C**), but 12-month-old SPF female 3xTg mice performed better than wildtype control mice (**Figure S11B**), consistent with a previous report [38]. Similarly, 5xFAD mice showed no deficits in Y-maze at 5 or 8 months of age (**Figure S11D and E**). We did not observe any deficits in object recognition in male or female 3xTg or 5xFAD mice (**Figure S12**), except for SPF 3xTg females at 7 months of age (**Figure S12A**) and GF 5xFAD males at 8 months of age (**Figure S12E**). Together, these data highlight deficits in spatial and working memory in the 3xTg and 5xFAD mouse models, with negligible effects on recognition memory. Our results support the notion that age, inflammatory state, sex, and the microbiome impact outcomes of cognitive performance, with the most significant effects by gut bacteria being on the interactions between sex and inflammation.

4 DISCUSSION

The microbiome is an important contributor to inflammation, and has recently been implicated in neurodegenerative disorders like AD [39–41]. Whether or how gut bacteria actively contribute to AD pathophysiology remains an open question. In this study, we examined immune and cognitive profiles in two transgenic mouse models of AD, in the presence or absence of a microbiome to understand how the microbiome shapes inflammation associated with AD. We found that the microbiome marginally influences the onset of inflammation in the brain-draining lymph nodes in the mouse models, but strongly modulates systemic immune responses, the cytokine response in local lymphoid tissues, and cognitive deficits. Notably, the inflammatory state in mice was modulated by sex, and this sex effect differed between local and systemic lymphoid tissues and between mice with an intact and absent microbiome.

In the 3xTg and 5xFAD mouse models, we found two contrasting inflammatory environments: (1) in 3xTg mice, inflammation was evident throughout secondary lymphoid tissues, including those associated with the intestine and brain, as well as systemically; (2) in 5xFAD mice, inflammation was more limited and, while somewhat systemic, largely localized to intestinal tissue and brain-draining lymph nodes. In both models, inflammation was driven by an activated adaptive immune response, with elevated $CD4^+$ T cells and B cells. However, as evident from the grossly enlarged spleens in 3xTg mice compared to the more mildly enlarged spleens of 5xFAD mice, 3xTg mice had a more pronounced inflammatory response. The most significant difference in the genetics between the models is expression of the tau protein, in addition to amyloid precursor protein and presenilin, in 3xTg mice, which result in both tau aggregation (tauopathy) and Aβ deposition [11]. The ectopic expression of human tau in mice has been shown to increase adaptive immune responses and brain atrophy in another AD model and may be a factor in the widespread immune responses we observed in 3xTg mice [42].

Previous studies have shown that the adaptive immunity participates in both protective and pathogenic processes in AD mouse models [43]. Complete abrogation of T and B cell responses in the 5xFAD model by genetic knockout of *Rag2 and Il2rg* results in increased amyloid aggregation and decreased brain expression of genes related to immunoglobulin antibody production and associated signaling, indicating a protective role for the adaptive immune system

[14]. Paradoxically, the loss of B cells alone results in reduced amyloid aggregation and improved cognitive function in 3xTg mice [15]. Studies indicate that B cell-produced autoantibodies are present in both the 3xTg and 5xFAD mouse models [26,28]. Chronic inflammatory states may contribute to pathogenic mechanisms that promote cellular stress, death, and the progression of AD. T and B cells, among other immune cells, have been shown to promote chronic inflammation through antibody production, activation of additional immune cells, and inflammatory cytokine production [15,43–45]. Adaptive immune responses were largely unchanged with age in 3xTg mice, in contrast to the attenuation of immune responses in 5xFAD mice. This indicates that chronic inflammation is present in 3xTg mice, which may contribute to more severe pathological outcomes.

Here, we find that the onset of inflammation in both the 3xTg and 5xFAD models was influenced by sex, with female mice showing earlier activation of adaptive immunity. This corresponds with a previously reported early rise in Aβ in the brains of female 3xTg and 5xFAD mice [11,46]. The cause of the accelerated pathology in female mice is not well understood. Previous studies suggest that pathology in the 3xTg and 5xFAD models is influenced by sex hormones, as alterations of sex hormones during early development and adulthood in 3xTg mice, or modulation of estrogen receptor activity in 5xFAD mice, can modify Aβ accumulation [22,47–49]. Notably in humans, an early study identified that estrogen-based hormone therapy reduced the risk of AD in women [50].

We observed elevated T and B cell counts and cytokine production in the draining lymph nodes of both the brain and intestine, indicating that immune responses may be activated and/or maintained by both brain and peripheral amyloid or tau pathology. There is significantly more (25x) Aβ peptide in the circulation of 3xTg compared to 5xFAD mice, which might contribute to the splenomegaly and hepatomegaly of 3xTg mice observed in this study and by others [26,27,51,52]. The liver, kidneys, spleen, and small intestine are important sites for the clearance of circulating Aβ and may act as hubs for activation of systemic immunity [53,54]. Previous work demonstrated reduced amyloid concentration in the brains of GF or antibiotic-treated mice [3–5]; therefore, our expectation was to find reduced systemic inflammation. Remarkably, while 3xTg female mice showed attenuated systemic immune responses under GF conditions, 3xTg

male mice had elevated T and B cell numbers. A previous study noted that male 3xTg mice develop a more robust autoimmune-like response, with serum antibodies against cell nuclei [29]. In 5xFAD mice, we observed reduced inflammation in GF conditions except for elevated cytokine responses in males. These findings suggest a sex- and microbiome-mediated effect on systemic inflammation which requires further study.

Inflammation corresponded with cognitive deficits in 3xTg and 5xFAD mice, an effect most pronounced in 3xTg female mice at early ages and in SPF conditions. Of note, GF 3xTg male mice had significant cognitive deficits, which corresponded with an increased systemic inflammatory response, suggesting that severe inflammatory responses may be associated with cognitive function, although the mechanism is not clear. 5xFAD mice indicated cognitive deficits at only the last time point measured (8 months), with deficits more pronounced in SPF than GF conditions.

Limitations of this work include variability in the results of cognitive testing and a limited scope of the immune response survey, restricted mainly to secondary lymphoid tissues and the adaptive immune response. Discrepancies in reported cognitive deficits exist across studies [23,25], perhaps due to technical differences between testing conditions, different microbiomes between animal facilities, or other variables. For immune response evaluation, we chose secondary lymphoid tissues because they represent hubs of immune activation. In future studies, local tissue responses may provide additional insight into the mechanisms of immune activation and resolution. In addition, only the intestinal tissue of 5xFAD mice was evaluated due to the specific increase in IL-17A^{+} T cells observed at this site.

In conclusion, we found that the microbiome influences both inflammatory and cognitive outcomes in a sex-dependent manner in two mouse models of AD. Inflammation was observed in both female and male mice and was attenuated in germ free conditions. Unexpectedly, GF male 3xTg mice maintained elevated adaptive immune and cytokine responses that correlated with cognitive deficits, indicating a protective role for the microbiome in male mice in this model. These data demonstrate a sex and microbiome interaction in the immune response and cognitive performance of AD mouse models. Future studies may focus on microbiome-influenced

mechanisms that intersect with sex hormones and immune responses to determine their effects on AD-like outcomes in mice, and perhaps in humans.

ACKNOWLEDGMENTS
We thank the Mazmanian laboratory for helpful suggestions to this work and Catherine Oikonomou for assistance with manuscript editing. We thank the Caltech Flow Cytometry and Cell Sorting Facility for flow cytometry services and assistance.

SOURCES OF FUNDING
The work was supported by the National Institutes of Health - Alzheimer's Gut Microbiome Project (1U19AG063744) and Heritage Medical Research Institute - Host-Microbial Symbiosis (HMRI-15-09-01). J.W.B. is supported by the Research and Outreach Fellowship awarded by the Caltech Biology and Biological Engineering Division.

DISCLOSURES
The authors declare no conflicts of interest.

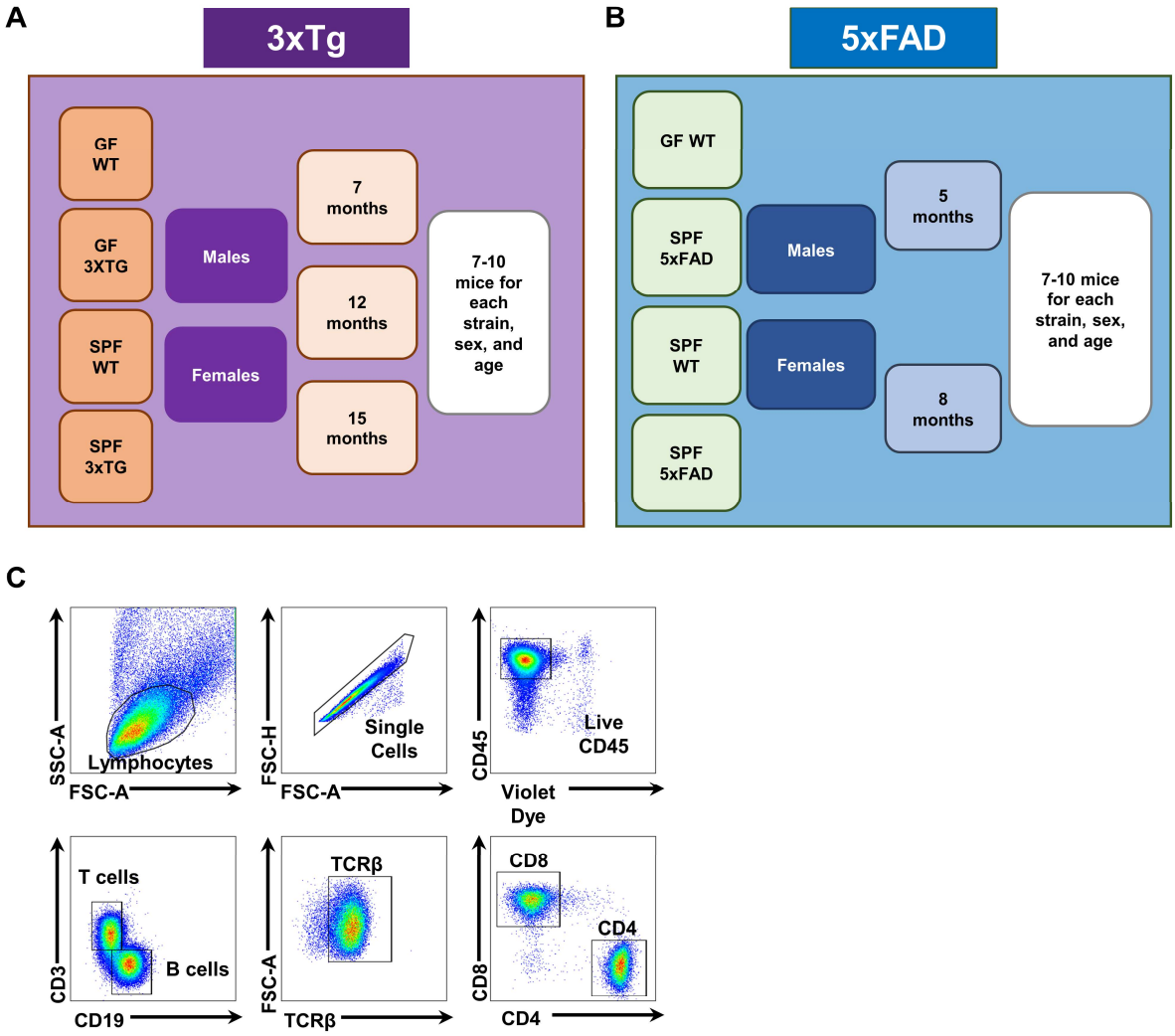

Supplemental Figure 1. Experimental design and flow cytometry gating.
(A) Illustration of experimental design for genotypes, housing conditions, ages, and sex for 3xTg and (B) 5xFAD mice. (C) Flow cytometry gating strategy for T and B cell analysis.

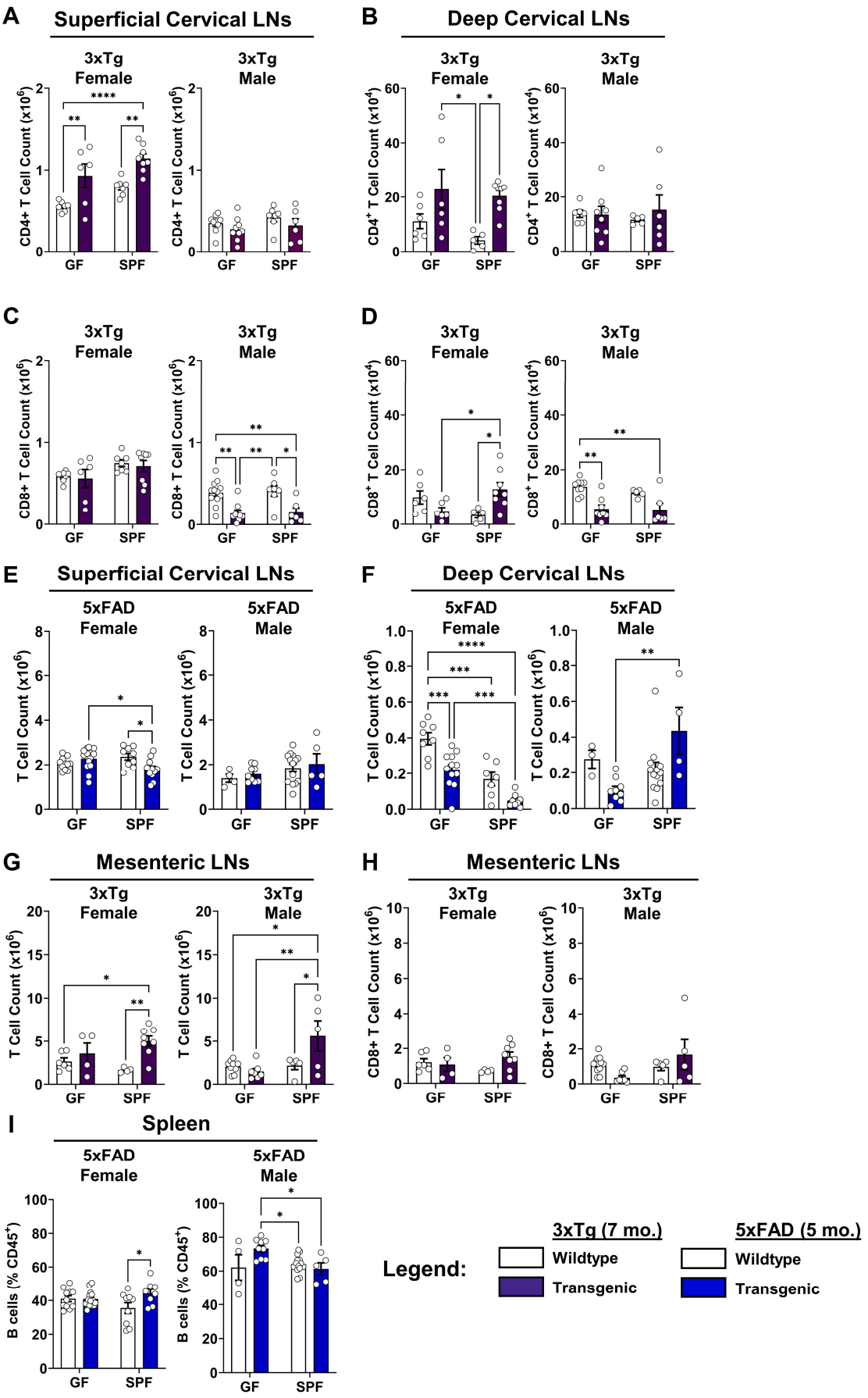
A
Superficial Cervical LNs
3xTg Female
3xTg Male
CD4+ T Cell Count (x10^6)
GF
SPF
B
Deep Cervical LNs
CD4+ T Cell Count (x10^4)
C
CD8+ T Cell Count (x10^6)
D
CD8+ T Cell Count (x10^4)
E
5xFAD Female
5xFAD Male
T Cell Count (x10^6)
F
G
Mesenteric LNs
H
I
Spleen
B cells (% CD45+)
Legend:
3xTg (7 mo.)
Wildtype
Transgenic
5xFAD (5 mo.)
Wildtype
Transgenic

Supplementary Figure 2. T and B cell immune responses in the 3xTg and 5xFAD models. (A) Quantification of $CD4^+$ T cell counts in the superficial cervical lymph nodes of female (Left) and male (Right) 3xTg mice compared to wildtype controls in germ-free (GF) and specific pathogen free (SPF) conditions at 7 months of age. (B) Deep cervical lymph nodes. (C) Quantification of $CD8^+$ T cell counts in the superficial cervical lymph nodes of female (Left) and male (Right) 3xTg mice at 7 months of age. (D) Deep cervical lymph nodes. Data are pooled from 2 independent experiments (n = 5 to 14 per group); two-way ANOVA. (E) Quantification of T cell counts in the superficial cervical lymph nodes of female (Left) and male (Right) 5xFAD mice at 5 months age. (F) Deep cervical lymph nodes. Data are pooled from 2 independent experiments (n = 3 to 14 per group); two-way ANOVA. (G) Quantification of T cell counts in the mesenteric lymph nodes of female (Left) and male (Right) 3xTg mice at 7 months of age. (H) Quantification of $CD8^+$ T cell counts. Data are pooled from 2 independent experiments (n = 4 to 11 per group); two-way ANOVA. (I) Quantification of B cell frequencies in the spleens of female (Right) and male (Left) 5xFAD mice at 5 months of age. Data are pooled from 2 independent experiments (n = 4 to 14 per group); two-way ANOVA. Error bars indicate SEM. *$P < 0.05$, **$P < 0.01$, ***$P < 0.001$, ****$P < 0.0001$; ns, not significant.

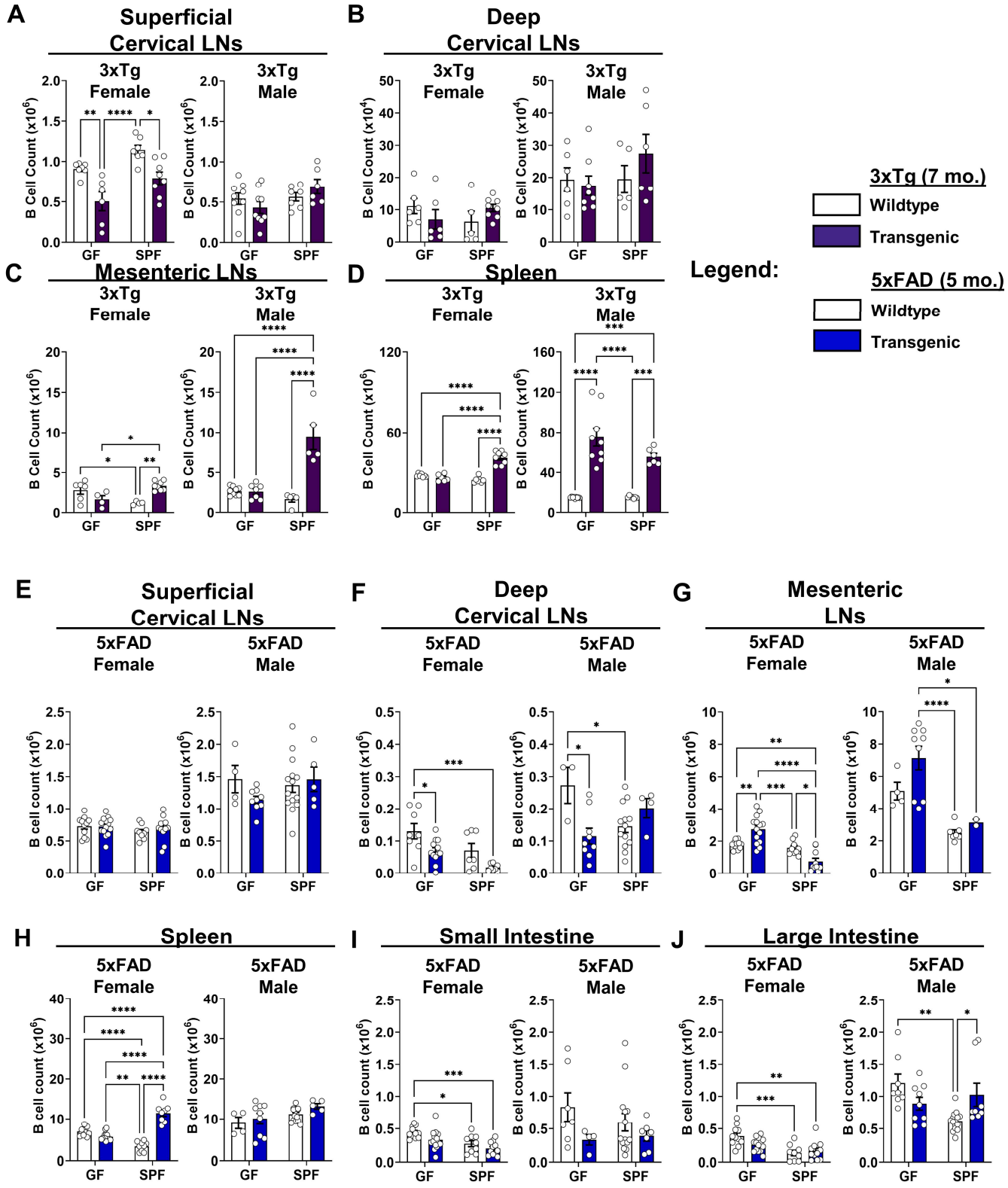
A
Superficial Cervical LNs
3xTg Female
3xTg Male
B Cell Count (x10^6)
GF
SPF
B
Deep Cervical LNs
B Cell Count (x10^4)
C
Mesenteric LNs
D
Spleen
Legend:
3xTg (7 mo.)
Wildtype
Transgenic
5xFAD (5 mo.)
Wildtype
Transgenic
E
Superficial Cervical LNs
5xFAD Female
5xFAD Male
B cell count (x10^6)
F
Deep Cervical LNs
G
Mesenteric LNs
H
Spleen
I
Small Intestine
J
Large Intestine

Supplementary Figure 3. B cell counts in 7-month-old 3xTg and 5-month-old 5xFAD mice. (A) Quantification of B cell counts in the superficial cervical lymph nodes of female (Left) and male (Right) 3xTg mice compared to wildtype controls in germ-free (GF) and specific pathogen free (SPF) conditions at 7 months of age. (B) Deep cervical lymph nodes. (C) Mesenteric lymph nodes. (D) Spleen. Data are pooled from 2 independent experiments (n = 4 to 14 per group); two-way ANOVA. (E) (A) Quantification of B cell counts in the superficial cervical lymph nodes of female (Left) and male (Right) 5xFAD mice compared to wildtype controls in germ-free (GF) and specific pathogen free (SPF) conditions at 5 months of age. (F) Deep cervical lymph nodes. (G) Mesenteric lymph nodes. (H) Spleen. (I) Small intestines. (J) Large intestines. Data are pooled from 2 independent experiments (n = 2 to 15 per group); two-way ANOVA. Error bars indicate SEM. *P < 0.05, **P < 0.01, ***P < 0.001, ****P < 0.0001; ns, not significant.

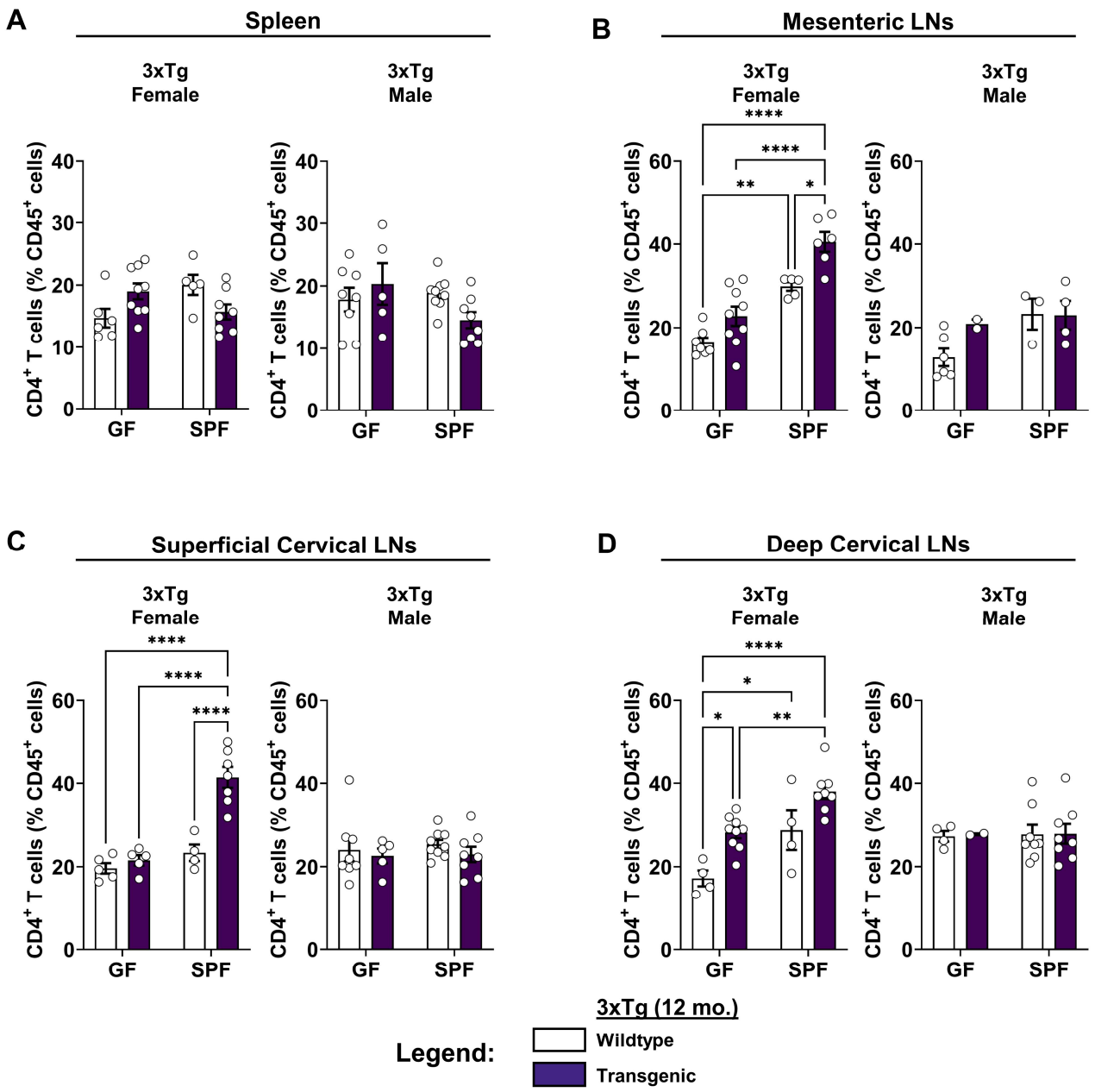

Supplementary Figure 4. Quantification of CD4$^+$ T cell frequencies in 12-month-old 3xTg mice.

(A) Quantification of CD4$^+$ T cell frequencies in the spleens of female (Left) and male (Right) 3xTg mice compared to wildtype controls in germ-free (GF) and specific pathogen free (SPF) conditions at 12 months of age. (B) Mesenteric lymph nodes. (C) Superficial cervical lymph nodes. (D) Deep cervical lymph nodes. Data are pooled from 2 independent experiments (n = 2 to 9 per group); two-way ANOVA. Error bars indicate SEM. *P < 0.05, **P < 0.01, ***P < 0.001, ****P < 0.0001; ns, not significant.

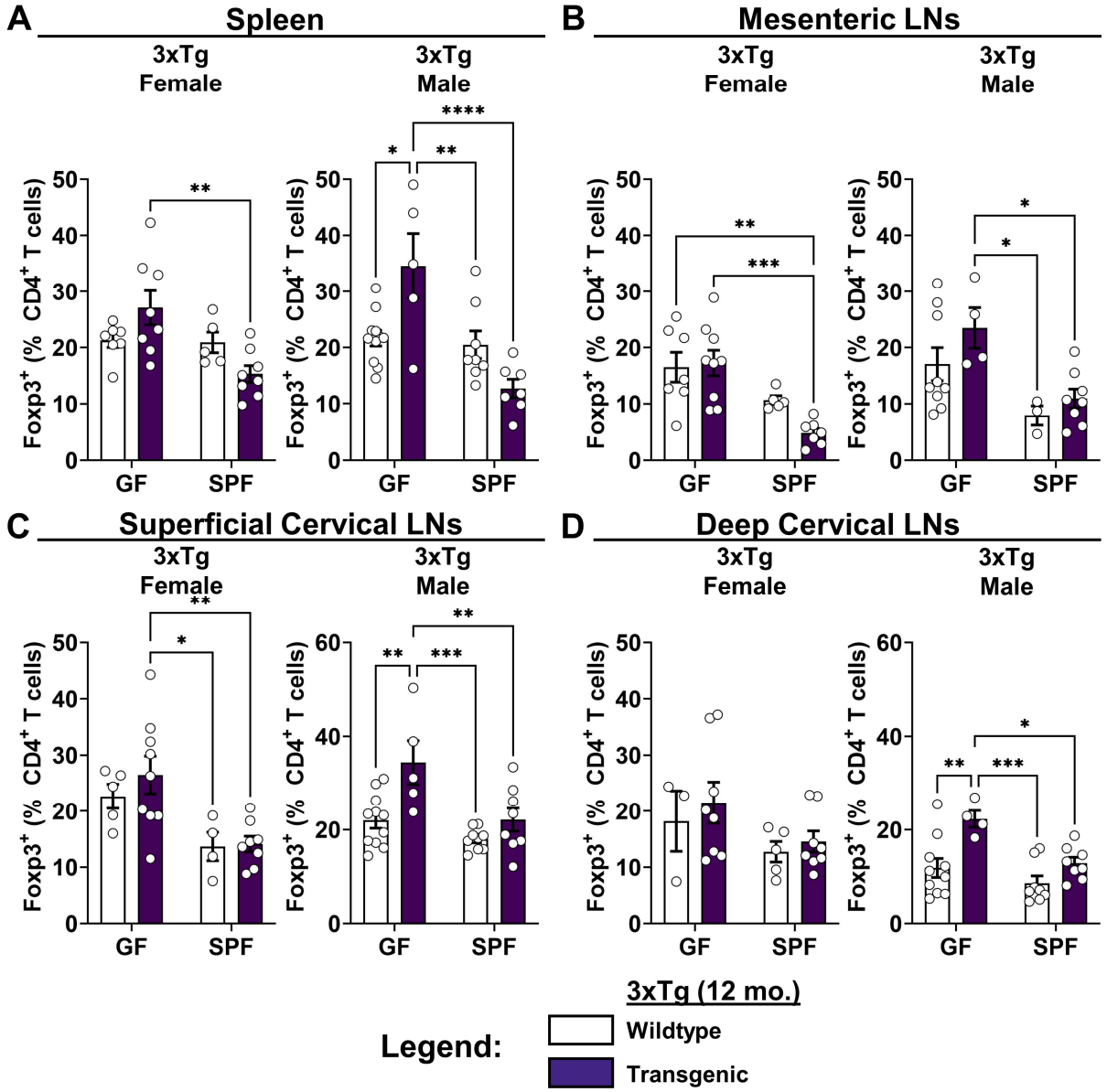

Supplementary Figure 5. Quantification of Foxp3$^+$ T cell frequencies in 12-month-old 3xTg mice.

(A) Quantification of Foxp3$^+$ T cell frequencies in the spleens of female (Left) and male (Right) 3xTg mice compared to wildtype controls in germ-free (GF) and specific pathogen free (SPF) conditions at 12 months of age. (B) Mesenteric lymph nodes. (C) Superficial cervical lymph nodes. (D) Deep cervical lymph nodes. Data are pooled from 2 independent experiments (n = 2 to 11 per group); two-way ANOVA. Error bars indicate SEM. *P < 0.05, **P < 0.01, ***P < 0.001, ****P < 0.0001; ns, not significant.

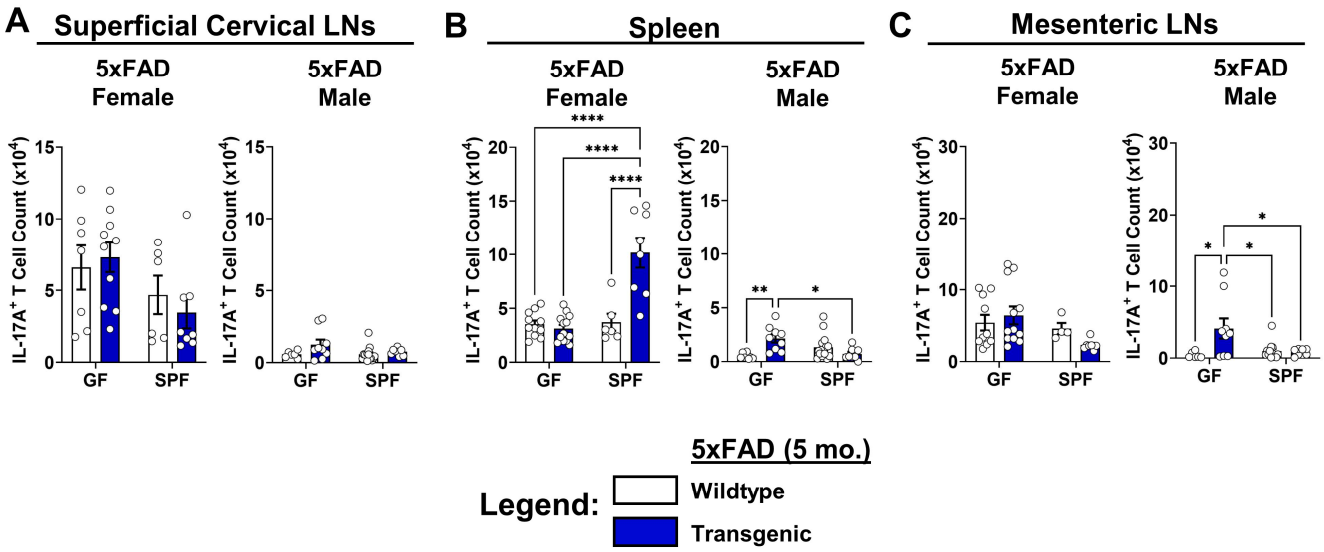

Supplementary Figure 6. IL-17A T cell counts in 5xFAD mice.
(A) Quantification of IL-17A^{+} T cell counts in the superficial cervical lymph nodes of female (Left) and male (Right) 5xFAD mice compared to wildtype controls in germ-free (GF) and specific pathogen free (SPF) conditions at 5 months of age. (B) Spleen. (C) Mesenteric lymph nodes. Data are pooled from 2 independent experiments (n = 4 to 15 per group); two-way ANOVA. Error bars indicate SEM. *P < 0.05, **P < 0.01, ***P < 0.001, ****P < 0.0001; ns, not significant.

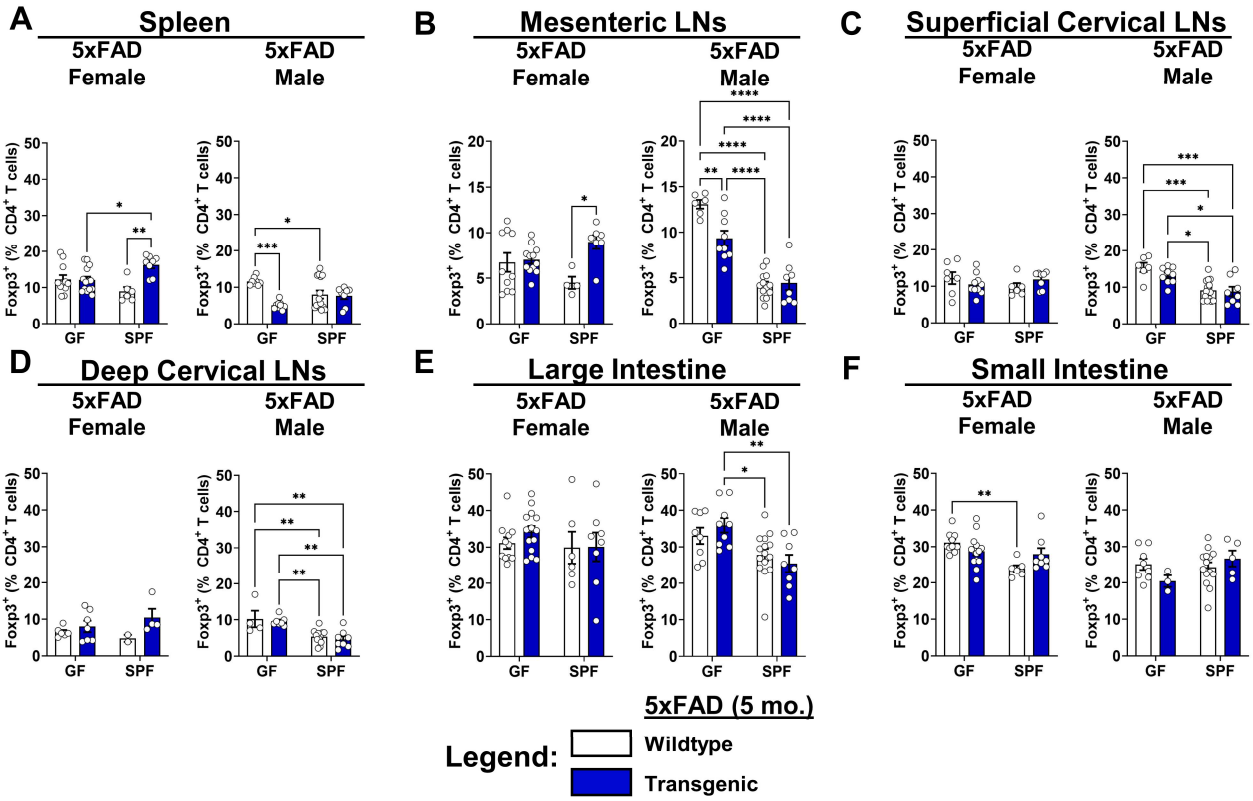

Supplementary Figure 7. Quantification of Foxp3$^+$ T cell frequencies in 5-month-old 5xFAD mice.

(A) Quantification of Foxp3$^+$ T cell frequencies in the spleens of female (Left) and male (Right) 5xFAD mice compared to wildtype controls in germ-free (GF) and specific pathogen free (SPF) conditions at 5 months of age. (B) Mesenteric lymph nodes. (C) Superficial cervical lymph nodes. (D) Deep cervical lymph nodes. (E) Large intestine. (F) Small intestine. Data are pooled from 2 independent experiments (n = 2 to 15 per group); two-way ANOVA. Error bars indicate SEM. *P < 0.05, **P < 0.01, ***P < 0.001, ****P < 0.0001; ns, not significant.

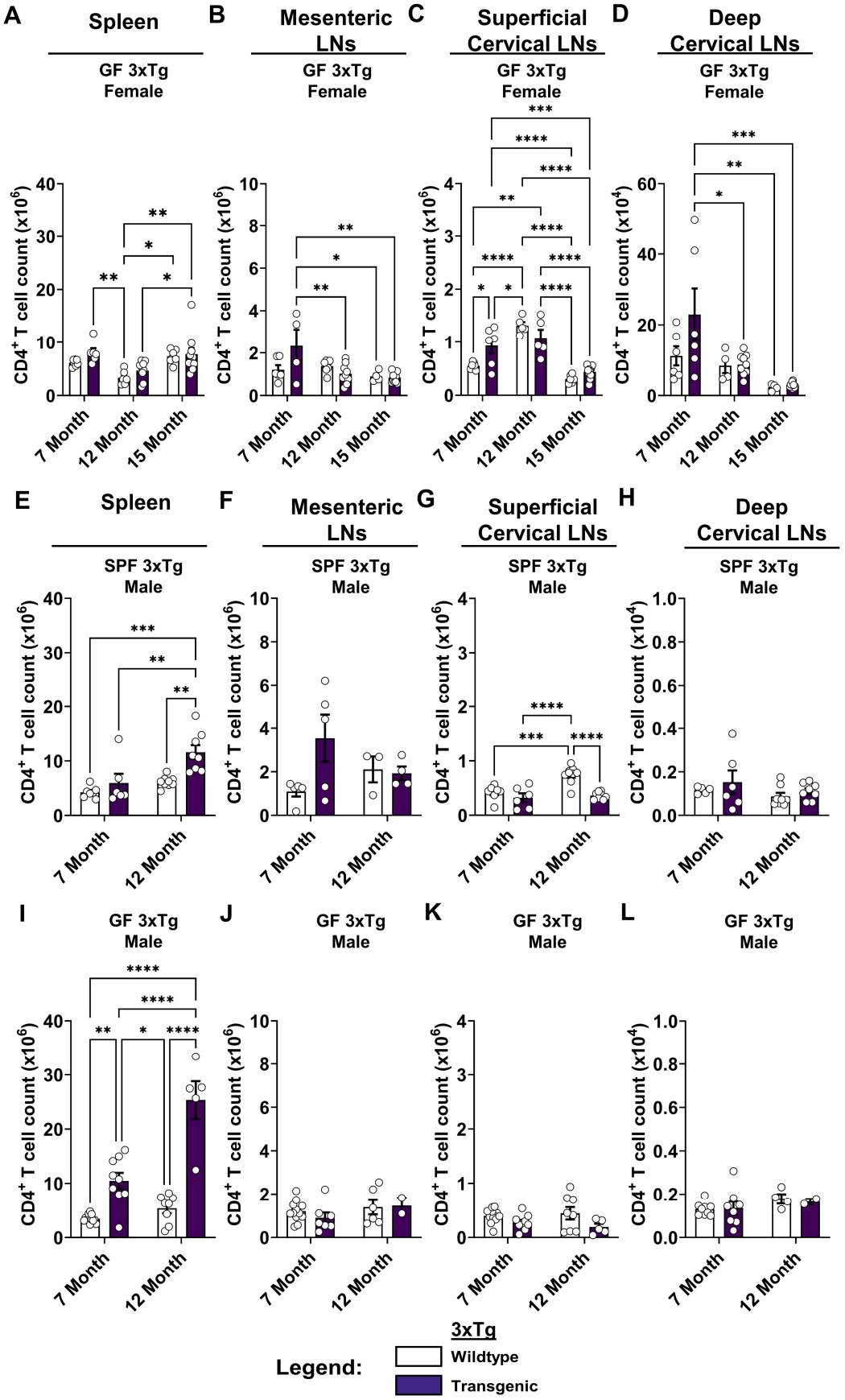
A
Spleen
GF 3xTg
Female
B
Mesenteric LNs
GF 3xTg
Female
C
Superficial Cervical LNs
GF 3xTg
Female
D
Deep Cervical LNs
GF 3xTg
Female
E
Spleen
SPF 3xTg
Male
F
Mesenteric LNs
SPF 3xTg
Male
G
Superficial Cervical LNs
SPF 3xTg
Male
H
Deep Cervical LNs
SPF 3xTg
Male
I
GF 3xTg
Male
J
GF 3xTg
Male
K
GF 3xTg
Male
L
GF 3xTg
Male
CD4+ T cell count (x10^6)
CD4+ T cell count (x10^4)
7 Month
12 Month
15 Month
Legend:
3xTg
Wildtype
Transgenic

Supplementary Figure 8. Longitudinal $CD4^+$ T cell responses in 3xTg mice.
(A) Quantification of $CD4^+$ T cell counts in the spleens of female 3xTg mice compared to wildtype controls in germ free (GF) conditions at 7-, 12-, and 15-month ages. (B) Mesenteric lymph nodes. (C) Superficial cervical lymph nodes. (D) Deep cervical lymph nodes. Data are pooled from 5 independent experiments (n = 4 to 10 per group); two-way ANOVA. (E) Quantification of $CD4^+$ T cell counts in the spleens of specific pathogen free (SPF) male 3xTg mice at 7-, 12-, and 15-month ages. (F) Mesenteric lymph nodes. (G) Superficial cervical lymph nodes. (H) Deep cervical lymph nodes. Data are pooled from 5 independent experiments (n = 3 to 9 per group); two-way ANOVA. (I) Quantification of $CD4^+$ T cell counts in the spleens of GF male 3xTg mice at 7-, 12-, and 15-month ages. (J) Mesenteric lymph nodes. (K) Superficial cervical lymph nodes. (L) Deep cervical lymph nodes. Data are pooled from 5 independent experiments (n = 2 to 9 per group); two-way ANOVA. Error bars indicate SEM. *P < 0.05, **P < 0.01, ***P < 0.001, ****P < 0.0001; ns, not significant.

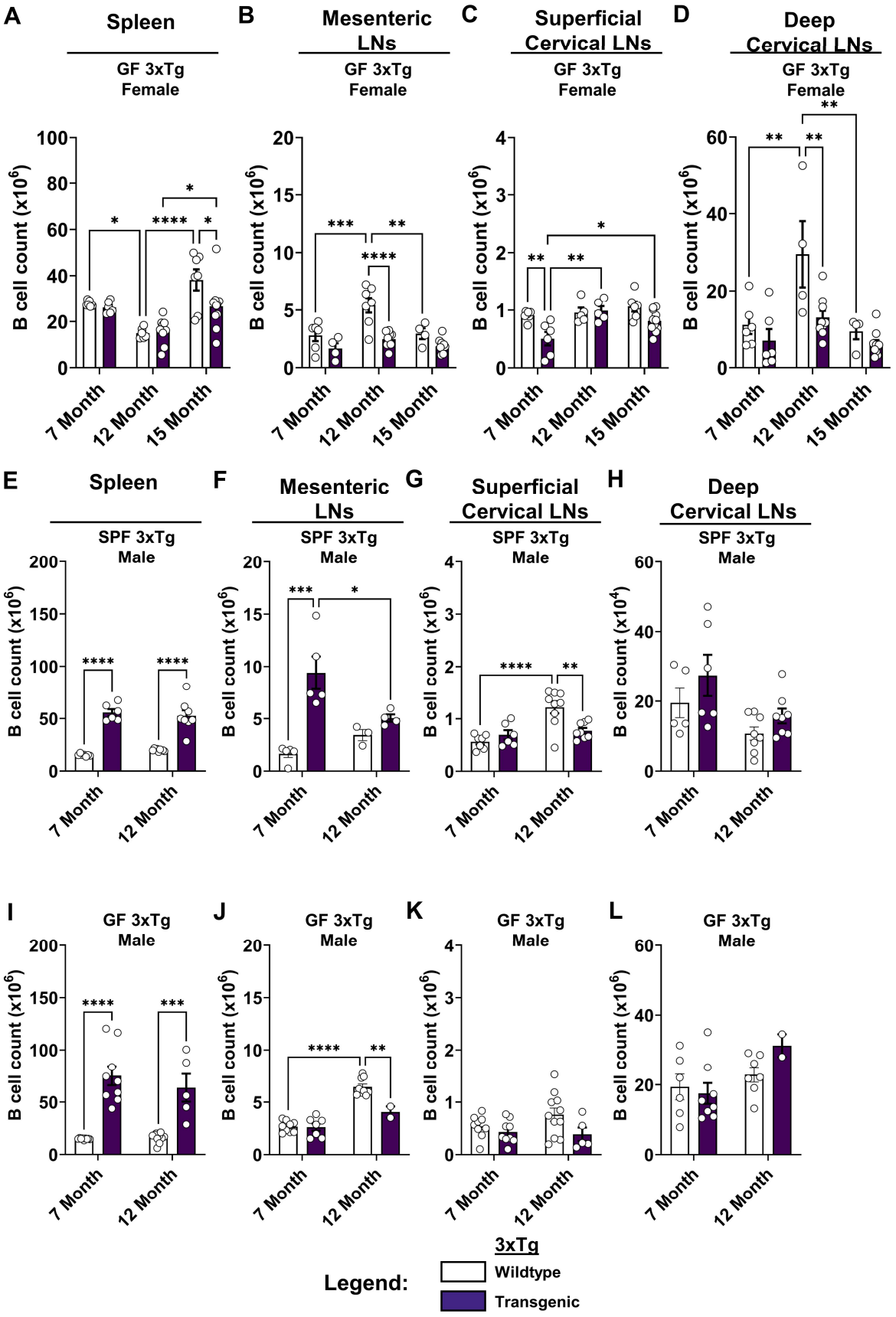
A
Spleen
GF 3xTg
Female
B
Mesenteric LNs
GF 3xTg
Female
C
Superficial Cervical LNs
GF 3xTg
Female
D
Deep Cervical LNs
GF 3xTg
Female
E
Spleen
SPF 3xTg
Male
F
Mesenteric LNs
SPF 3xTg
Male
G
Superficial Cervical LNs
SPF 3xTg
Male
H
Deep Cervical LNs
SPF 3xTg
Male
I
GF 3xTg
Male
J
GF 3xTg
Male
K
GF 3xTg
Male
L
GF 3xTg
Male
B cell count (x10^6)
B cell count (x10^4)
7 Month
12 Month
15 Month
Legend:
3xTg
Wildtype
Transgenic

Supplementary Figure 9. Longitudinal B cell responses in 3xTg mice.
(A) Quantification of B cell counts in the spleens of female 3xTg mice compared to wildtype controls in germ free (GF) conditions at 7-, 12-, and 15-month ages. (B) Mesenteric lymph nodes. (C) Superficial cervical lymph nodes. (D) Deep cervical lymph nodes. Data are pooled from 5 independent experiments (n = 4 to 10 per group); two-way ANOVA. (E) Quantification of B cell counts in the spleens of specific pathogen free (SPF) male 3xTg mice at 7-, 12-, and 15-month ages. (F) Mesenteric lymph nodes. (G) Superficial cervical lymph nodes. (H) Deep cervical lymph nodes. Data are pooled from 5 independent experiments (n = 3 to 9 per group); two-way ANOVA. (I) Quantification of B cell counts in the spleens of GF male 3xTg mice at 7-, 12-, and 15-month ages. (J) Mesenteric lymph nodes. (K) Superficial cervical lymph nodes. (L) Deep cervical lymph nodes. Data are pooled from 5 independent experiments (n = 2 to 11 per group); two-way ANOVA. For clarity, only significant comparisons of the same mouse group between ages or between transgenic and control mice at the same age are shown. Error bars indicate SEM. *P < 0.05, **P < 0.01, ***P < 0.001, ****P < 0.0001; ns, not significant.

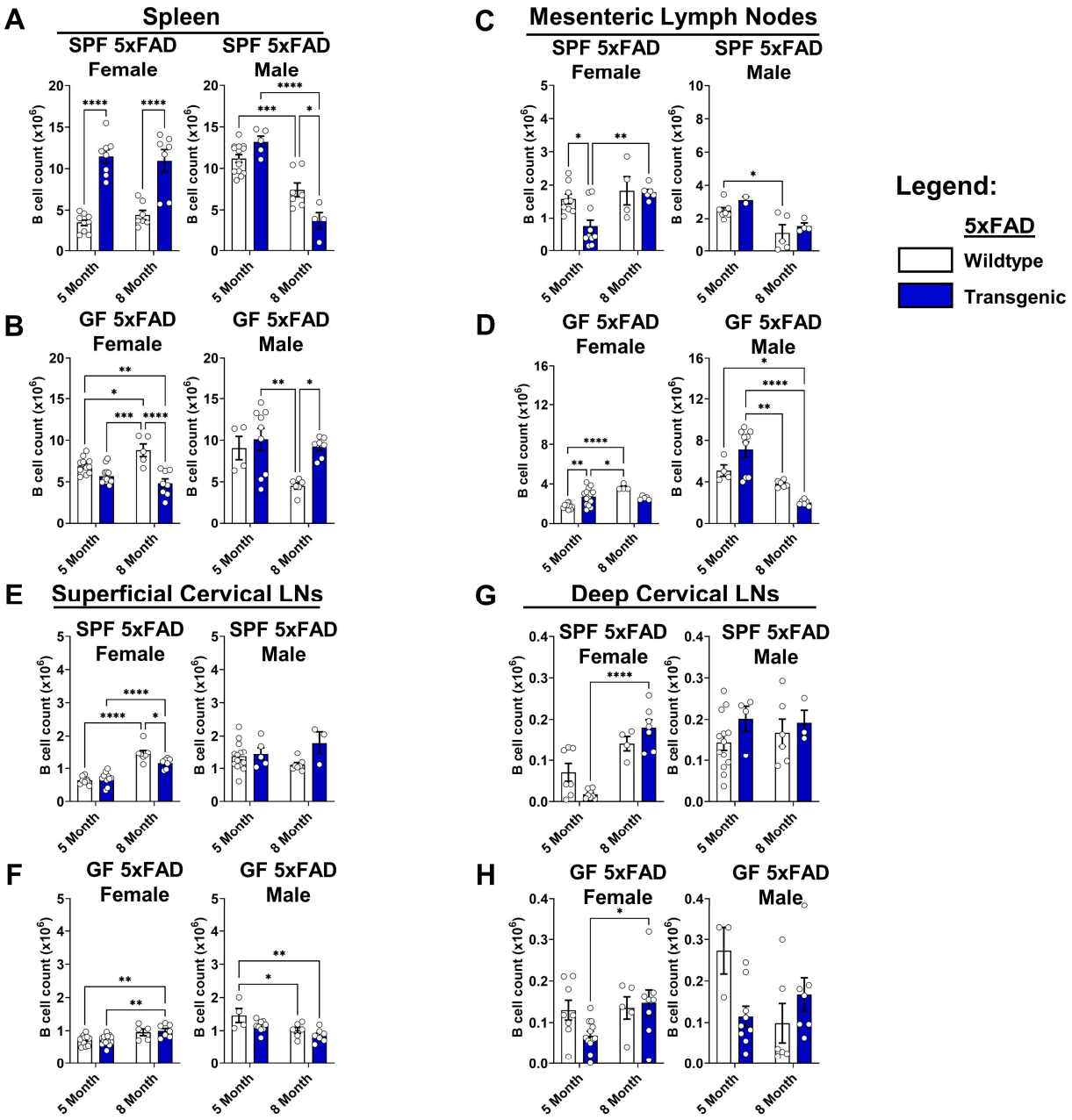

Supplementary Figure 10. Longitudinal B cell responses in 5xFAD mice.
(A) Quantification of B cell counts in the spleens of female (Left) and male (Right) 5xFAD mice compared to wildtype controls specific pathogen free (SPF) and (B) Germ-free (GF) conditions at 5 and 8 months of age. (C) Mesenteric lymph nodes in SPF and (D) GF conditions. (E) Superficial cervical lymph nodes in SPF and (F) GF conditions. (G) Deep cervical lymph nodes in SPF and (H) GF conditions. Data are pooled from 2 independent experiments (n = 2 to 15 per group); two-way ANOVA. For clarity, only significant comparisons of the same mouse group between ages or between transgenic and control mice at the same age are shown. Error bars indicate SEM. *P < 0.05, **P < 0.01, ***P < 0.001, ****P < 0.0001; ns, not significant.

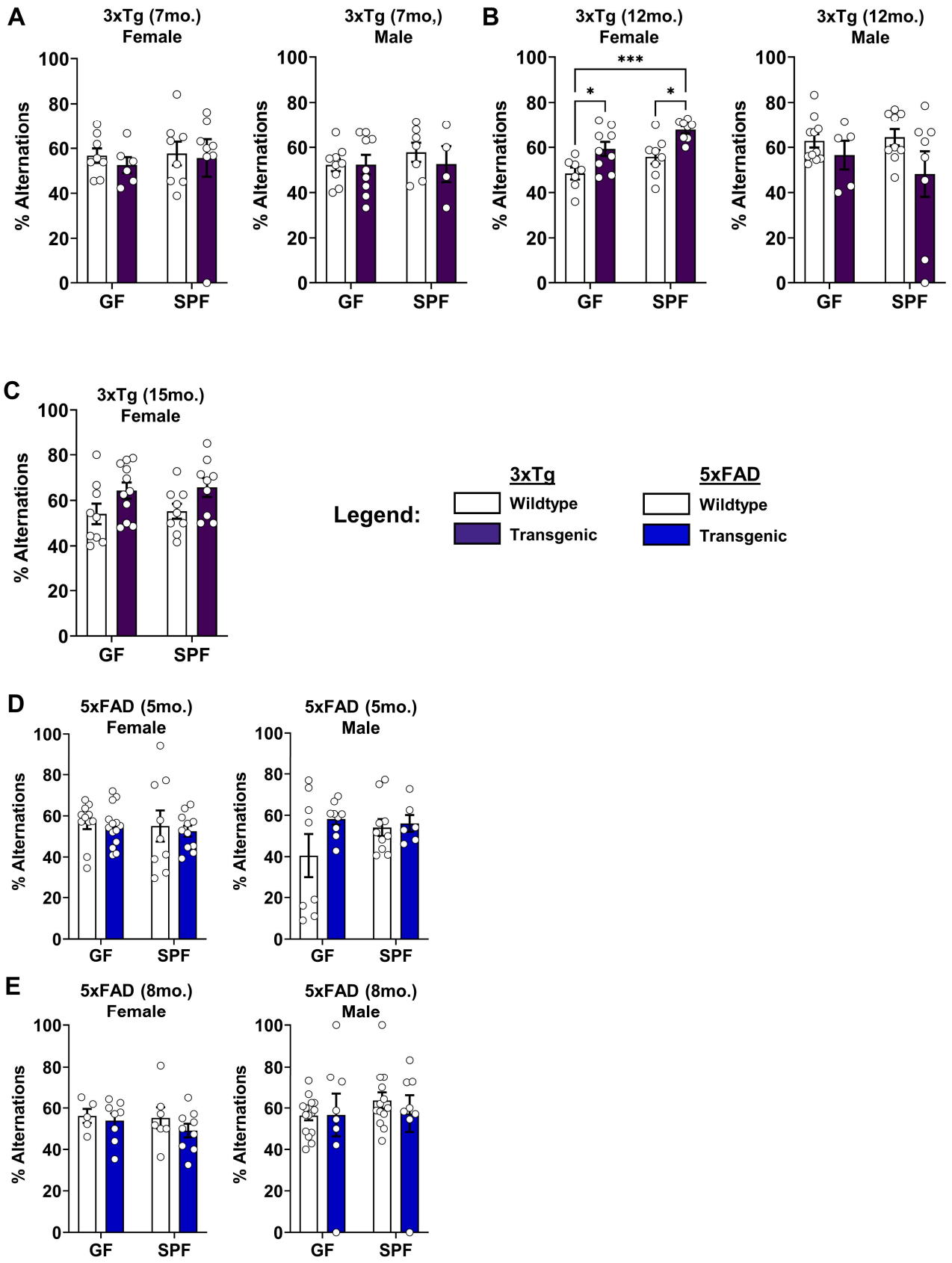
A
3xTg (7mo.)
Female
3xTg (7mo,)
Male
B
3xTg (12mo.)
Female
3xTg (12mo.)
Male
C
3xTg (15mo.)
Female
D
5xFAD (5mo.)
Female
5xFAD (5mo.)
Male
E
5xFAD (8mo.)
Female
5xFAD (8mo.)
Male
% Alternations
GF
SPF
***
*
*
Legend:
3xTg
Wildtype
Transgenic
5xFAD
Wildtype
Transgenic

Supplementary Figure 11. Cognitive deficits in Y-maze testing of female and male 7-, 12- and 15-month-old 3xTg and 5- and 8-month-old 5xFAD mice.
(A) Alternations (%) in Y-maze testing for cognitive deficits in 7-month-old female (Left) and male (Right) 3xTg mice compared to wildtype controls in germ free (GF) or specific pathogen free (SPF) conditions. (B) 12-month-old female (Left) and male (Right) 3xTg mice. (C) 15-month-old female 3xTg mice. Data are pooled from 2 independent experiments (n = 5 to 14 per group); two-way ANOVA. (D) Alternations (%) in Y-maze testing for cognitive deficits in 5-month-old female (Left) and male (Right) 5xFAD. (E) 8-month-old female (Left) and male (Right) 5xFAD mice. Data are pooled from 2 independent experiments (n = 5 to 16 per group); two-way ANOVA. Error bars indicate SEM. *P < 0.05, **P < 0.01, ***P < 0.001, ****P < 0.0001; ns, not significant.

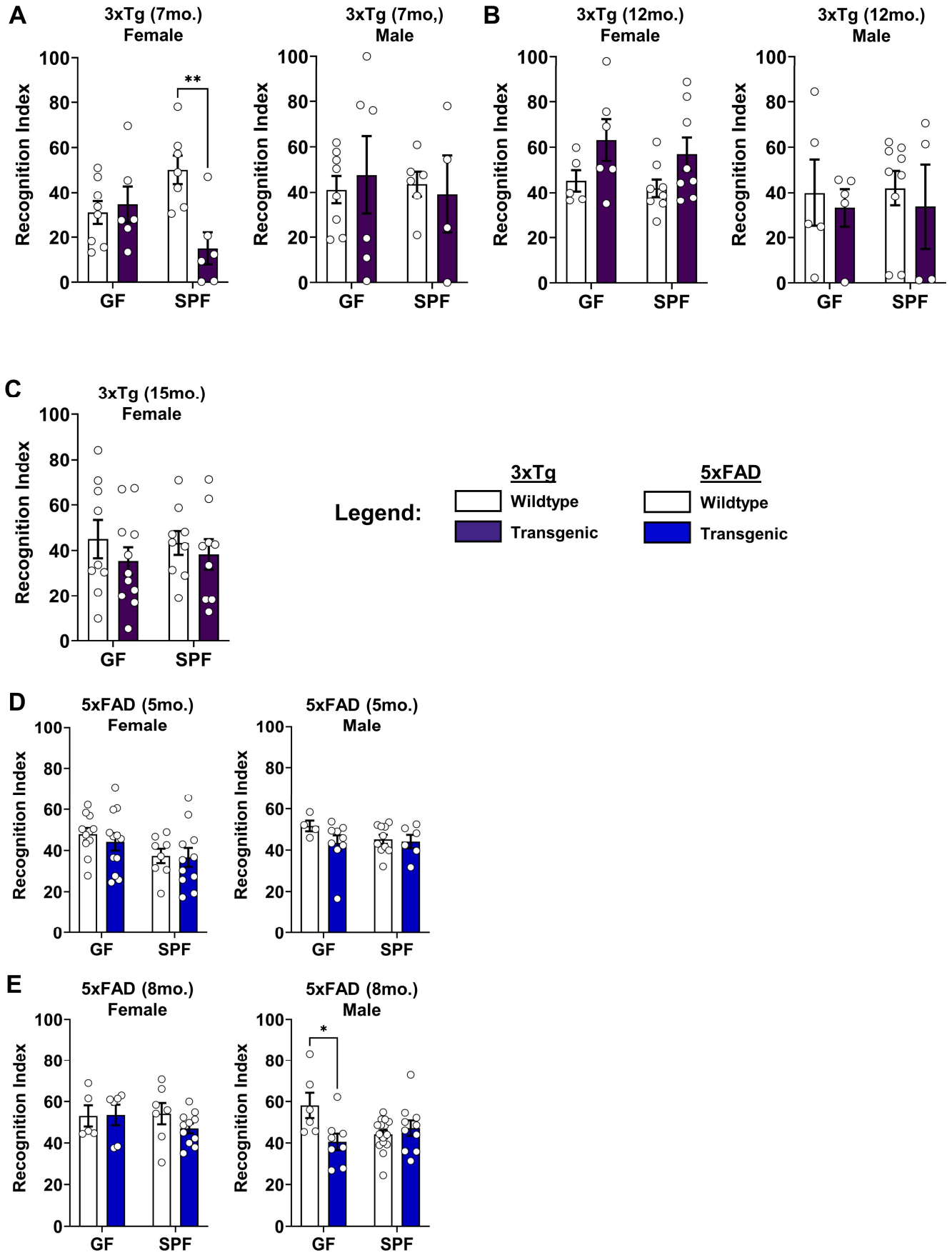
A
3xTg (7mo.)
Female
3xTg (7mo,)
Male
B
3xTg (12mo.)
Female
3xTg (12mo.)
Male
C
3xTg (15mo.)
Female
D
5xFAD (5mo.)
Female
5xFAD (5mo.)
Male
E
5xFAD (8mo.)
Female
5xFAD (8mo.)
Male
Recognition Index
0
20
40
60
80
100
GF
SPF
**
*
Legend:
3xTg
Wildtype
Transgenic
5xFAD
Wildtype
Transgenic

Supplementary Figure 12. Cognitive deficits in Novel Object Recognition (NOR) testing of female and male 7-, 12- and 15-month-old 3xTg and 5- and 8-month-old 5xFAD mice.
(A) Recognition index as measured in novel object recognition testing for cognitive deficits in 7-month-old female (Left) and male (Right) 3xTg mice compared to wildtype controls in germ free (GF) or specific pathogen free (SPF) conditions. (B) 12-month-old female (Left) and male (Right) 3xTg mice. (C) 15-month-old female 3xTg mice. Data are pooled from 2 independent experiments (n = 4 to 14 per group); two-way ANOVA. (D) Recognition index as measured in novel object recognition testing for cognitive deficits in 5-month-old female (Left) and male (Right) 5xFAD mice. (E) 8-month-old female (Left) and male (Right) 5xFAD mice. Data are pooled from 2 independent experiments (n = 5 to 16 per group); two-way ANOVA. Error bars indicate SEM. *P < 0.05, **P < 0.01, ***P < 0.001, ****P < 0.0001; ns, not significant.

REFERENCES

[1] 2023 Alzheimer's disease facts and figures. Alzheimers Dement 2023;19:1598–695. https://doi.org/10.1002/alz.13016.

[2] Andrews SJ, Renton AE, Fulton-Howard B, Podlesny-Drabiniok A, Marcora E, Goate AM. The complex genetic architecture of Alzheimer's disease: novel insights and future directions. eBioMedicine 2023;90:104511. https://doi.org/10.1016/j.ebiom.2023.104511.

[3] Minter MR, Zhang C, Leone V, Ringus DL, Zhang X, Oyler-Castrillo P, et al. Antibiotic-induced perturbations in gut microbial diversity influences neuro-inflammation and amyloidosis in a murine model of Alzheimer's disease. Sci Rep 2016;6:30028. https://doi.org/10.1038/srep30028.

[4] Minter MR, Hinterleitner R, Meisel M, Zhang C, Leone V, Zhang X, et al. Antibiotic-induced perturbations in microbial diversity during post-natal development alters amyloid pathology in an aged APPSWE/PS1ΔE9 murine model of Alzheimer's disease. Sci Rep 2017;7:10411. https://doi.org/10.1038/s41598-017-11047-w.

[5] Harach T, Marungruang N, Duthilleul N, Cheatham V, Mc Coy KD, Frisoni G, et al. Reduction of Abeta amyloid pathology in APPPS1 transgenic mice in the absence of gut microbiota. Sci Rep 2017;7:41802. https://doi.org/10.1038/srep41802.

[6] Seo D, Holtzman DM. Current understanding of the Alzheimer's disease-associated microbiome and therapeutic strategies. Exp Mol Med 2024;56:86–94. https://doi.org/10.1038/s12276-023-01146-2.

[7] Wang X, Sun G, Feng T, Zhang J, Huang X, Wang T, et al. Sodium oligomannate therapeutically remodels gut microbiota and suppresses gut bacterial amino acids-shaped neuroinflammation to inhibit Alzheimer's disease progression. Cell Res 2019;29:787–803. https://doi.org/10.1038/s41422-019-0216-x.

[8] Walker JM, Dixit S, Saulsberry AC, May JM, Harrison FE. Reversal of high fat diet-induced obesity improves glucose tolerance, inflammatory response, β-amyloid accumulation and cognitive decline in the APP/PSEN1 mouse model of Alzheimer's disease. Neurobiol Dis 2017;100:87–98. https://doi.org/10.1016/j.nbd.2017.01.004.

[9] Oddo S, Caccamo A, Shepherd JD, Murphy MP, Golde TE, Kayed R, et al. Triple-Transgenic Model of Alzheimer's Disease with Plaques and Tangles. Neuron 2003;39:409–21. https://doi.org/10.1016/S0896-6273(03)00434-3.

[10] Oakley H, Cole SL, Logan S, Maus E, Shao P, Craft J, et al. Intraneuronal β-Amyloid Aggregates, Neurodegeneration, and Neuron Loss in Transgenic Mice with Five Familial Alzheimer's Disease Mutations: Potential Factors in Amyloid Plaque Formation. J Neurosci 2006;26:10129–40. https://doi.org/10.1523/JNEUROSCI.1202-06.2006.

[11] Javonillo DI, Tran KM, Phan J, Hingco E, Kramár EA, Da Cunha C, et al. Systematic Phenotyping and Characterization of the 3xTg-AD Mouse Model of Alzheimer's Disease. Front Neurosci 2022;15:785276. https://doi.org/10.3389/fnins.2021.785276.

[12] Newcombe EA, Camats-Perna J, Silva ML, Valmas N, Huat TJ, Medeiros R. Inflammation: the link between comorbidities, genetics, and Alzheimer's disease. J Neuroinflammation 2018;15:276. https://doi.org/10.1186/s12974-018-1313-3.

[13] Shi Y, Holtzman DM. Interplay between innate immunity and Alzheimer disease: APOE and TREM2 in the spotlight. Nat Rev Immunol 2018;18:759–72. https://doi.org/10.1038/s41577-018-0051-1.

[14] Marsh SE, Abud EM, Lakatos A, Karimzadeh A, Yeung ST, Davtyan H, et al. The adaptive immune system restrains Alzheimer's disease pathogenesis by modulating microglial function. Proc Natl Acad Sci 2016;113. https://doi.org/10.1073/pnas.1525466113.

[15] Kim K, Wang X, Ragonnaud E, Bodogai M, Illouz T, DeLuca M, et al. Therapeutic B-cell depletion reverses progression of Alzheimer's disease. Nat Commun 2021;12:2185. https://doi.org/10.1038/s41467-021-22479-4.

[16] Zhang Y, Shen Y, Liufu N, Liu L, Li W, Shi Z, et al. Transmission of Alzheimer's disease-associated microbiota dysbiosis and its impact on cognitive function: evidence from mice and patients. Mol Psychiatry 2023;28:4421–37. https://doi.org/10.1038/s41380-023-02216-7.

[17] Bostick JW, Schonhoff AM, Mazmanian SK. Gut microbiome-mediated regulation of neuroinflammation. Curr Opin Immunol 2022;76:102177. https://doi.org/10.1016/j.coi.2022.102177.

[18] Needham BD, Kaddurah-Daouk R, Mazmanian SK. Gut microbial molecules in behavioural and neurodegenerative conditions. Nat Rev Neurosci 2020;21:717–31. https://doi.org/10.1038/s41583-020-00381-0.

[19] Prieur EAK, Jadavji NM. Assessing Spatial Working Memory Using the Spontaneous Alternation Y-maze Test in Aged Male Mice. Bio-Protoc 2019;9:e3162. https://doi.org/10.21769/BioProtoc.3162.

[20] Leger M, Quiedeville A, Bouet V, Haelewyn B, Boulouard M, Schumann-Bard P, et al. Object recognition test in mice. Nat Protoc 2013;8:2531–7. https://doi.org/10.1038/nprot.2013.155.

[21] Attar A, Liu T, Chan W-TC, Hayes J, Nejad M, Lei K, et al. A Shortened Barnes Maze Protocol Reveals Memory Deficits at 4-Months of Age in the Triple-Transgenic Mouse Model of Alzheimer's Disease. PLoS ONE 2013;8:e80355. https://doi.org/10.1371/journal.pone.0080355.

[22] Carroll JC, Rosario ER, Kreimer S, Villamagna A, Gentzschein E, Stanczyk FZ, et al. Sex differences in β-amyloid accumulation in 3xTg-AD mice: Role of neonatal sex steroid hormone exposure. Brain Res 2010;1366:233–45. https://doi.org/10.1016/j.brainres.2010.10.009.

[23] Creighton SD, Mendell AL, Palmer D, Kalisch BE, MacLusky NJ, Prado VF, et al. Dissociable cognitive impairments in two strains of transgenic Alzheimer's disease mice revealed by a battery of object-based tests. Sci Rep 2019;9:57. https://doi.org/10.1038/s41598-018-37312-0.

[24] Dennison JL, Ricciardi NR, Lohse I, Volmar C-H, Wahlestedt C. Sexual Dimorphism in the 3xTg-AD Mouse Model and Its Impact on Pre-Clinical Research. J Alzheimers Dis 2021;80:41–52. https://doi.org/10.3233/JAD-201014.

[25] Brigas HC, Ribeiro M, Coelho JE, Gomes R, Gomez-Murcia V, Carvalho K, et al. IL-17 triggers the onset of cognitive and synaptic deficits in early stages of Alzheimer's disease. Cell Rep 2021;36:109574. https://doi.org/10.1016/j.celrep.2021.109574.

[26] Marchese M, Cowan D, Head E, Ma D, Karimi K, Ashthorpe V, et al. Autoimmune Manifestations in the 3xTg-AD Model of Alzheimer's Disease. J Alzheimers Dis 2014;39:191–210. https://doi.org/10.3233/JAD-131490.

[27] Yang S-H, Kim J, Lee MJ, Kim Y. Abnormalities of plasma cytokines and spleen in senile APP/PS1/Tau transgenic mouse model. Sci Rep 2015;5:15703. https://doi.org/10.1038/srep15703.

[28] Dinkins MB, Dasgupta S, Wang G, Zhu G, He Q, Kong JN, et al. The 5XFAD Mouse Model of Alzheimer's Disease Exhibits an Age-Dependent Increase in Anti-Ceramide IgG and Exogenous Administration of Ceramide Further Increases Anti-Ceramide Titers and Amyloid Plaque Burden. J Alzheimers Dis 2015;46:55–61. https://doi.org/10.3233/JAD-150088.

[29] Kapadia M, Mian MF, Michalski B, Azam AB, Ma D, Salwierz P, et al. Sex-Dependent Differences in Spontaneous Autoimmunity in Adult 3xTg-AD Mice. J Alzheimers Dis 2018;63:1191–205. https://doi.org/10.3233/JAD-170779.

[30] Mills KHG. IL-17 and IL-17-producing cells in protection versus pathology. Nat Rev Immunol 2023;23:38–54. https://doi.org/10.1038/s41577-022-00746-9.

[31] Pandiyan P, Bhaskaran N, Zou M, Schneider E, Jayaraman S, Huehn J. Microbiome Dependent Regulation of Tregs and Th17 Cells in Mucosa. Front Immunol 2019;10:426. https://doi.org/10.3389/fimmu.2019.00426.

[32] McGinley AM, Sutton CE, Edwards SC, Leane CM, DeCourcey J, Teijeiro A, et al. Interleukin-17A Serves a Priming Role in Autoimmunity by Recruiting IL-1β-Producing Myeloid Cells that Promote Pathogenic T Cells. Immunity 2020;52:342-356.e6. https://doi.org/10.1016/j.immuni.2020.01.002.

[33] Benakis C, Brea D, Caballero S, Faraco G, Moore J, Murphy M, et al. Commensal microbiota affects ischemic stroke outcome by regulating intestinal γδ T cells. Nat Med 2016;22:516–23. https://doi.org/10.1038/nm.4068.

[34] Smigiel KS, Srivastava S, Stolley JM, Campbell DJ. Regulatory T-cell homeostasis: steady-state maintenance and modulation during inflammation. Immunol Rev 2014;259:40–59. https://doi.org/10.1111/imr.12170.

[35] Sakaguchi S, Yamaguchi T, Nomura T, Ono M. Regulatory T Cells and Immune Tolerance. Cell 2008;133:775–87. https://doi.org/10.1016/j.cell.2008.05.009.

[36] Saksida T, Koprivica I, Vujičić M, Stošić-Grujičić S, Perović M, Kanazir S, et al. Impaired IL-17 Production in Gut-Residing Immune Cells of 5xFAD Mice with Alzheimer's Disease Pathology. J Alzheimers Dis 2017;61:619–30. https://doi.org/10.3233/JAD-170538.

[37] Sutton CE, Lalor SJ, Sweeney CM, Brereton CF, Lavelle EC, Mills KHG. Interleukin-1 and IL-23 Induce Innate IL-17 Production from γδ T Cells, Amplifying Th17 Responses and Autoimmunity. Immunity 2009;31:331–41. https://doi.org/10.1016/j.immuni.2009.08.001.

[38] Stover KR, Campbell MA, Van Winssen CM, Brown RE. Early detection of cognitive deficits in the 3xTg-AD mouse model of Alzheimer's disease. Behav Brain Res 2015;289:29–38. https://doi.org/10.1016/j.bbr.2015.04.012.

[39] Morais LH, Schreiber HL, Mazmanian SK. The gut microbiota–brain axis in behaviour and brain disorders. Nat Rev Microbiol 2021;19:241–55. https://doi.org/10.1038/s41579-020-00460-0.

[40] De Luca F, Shoenfeld Y. The microbiome in autoimmune diseases. Clin Exp Immunol 2018;195:74–85. https://doi.org/10.1111/cei.13158.

[41] Fan Y, Pedersen O. Gut microbiota in human metabolic health and disease. Nat Rev Microbiol 2021;19:55–71. https://doi.org/10.1038/s41579-020-0433-9.

[42] Chen X, Firulyova M, Manis M, Herz J, Smirnov I, Aladyeva E, et al. Microglia-mediated T cell infiltration drives neurodegeneration in tauopathy. Nature 2023;615:668–77. https://doi.org/10.1038/s41586-023-05788-0.

[43] Chen X, Holtzman DM. Emerging roles of innate and adaptive immunity in Alzheimer's disease. Immunity 2022;55:2236–54. https://doi.org/10.1016/j.immuni.2022.10.016.

[44] Sabatino JJ, Pröbstel A-K, Zamvil SS. B cells in autoimmune and neurodegenerative central nervous system diseases. Nat Rev Neurosci 2019;20:728–45. https://doi.org/10.1038/s41583-019-0233-2.

[45] Häusser-Kinzel S, Weber MS. The Role of B Cells and Antibodies in Multiple Sclerosis, Neuromyelitis Optica, and Related Disorders. Front Immunol 2019;10:201. https://doi.org/10.3389/fimmu.2019.00201.

[46] Forner S, Kawauchi S, Balderrama-Gutierrez G, Kramár EA, Matheos DP, Phan J, et al. Systematic phenotyping and characterization of the 5xFAD mouse model of Alzheimer's disease. Sci Data 2021;8:270. https://doi.org/10.1038/s41597-021-01054-y.

[47] Carroll JC, Rosario ER, Chang L, Stanczyk FZ, Oddo S, LaFerla FM, et al. Progesterone and Estrogen Regulate Alzheimer-Like Neuropathology in Female 3xTg-AD Mice. J Neurosci 2007;27:13357–65. https://doi.org/10.1523/JNEUROSCI.2718-07.2007.

[48] Farkas S, Szabó A, Török B, Sólyomvári C, Fazekas CL, Bánrévi K, et al. Ovariectomy-induced hormone deprivation aggravates Aβ1-42 deposition in the basolateral amygdala and cholinergic fiber loss in the cortex but not cognitive behavioral symptoms in a triple transgenic mouse model of Alzheimer's disease. Front Endocrinol 2022;13:985424. https://doi.org/10.3389/fendo.2022.985424.

[49] Quinn JF, Kelly MJ, Harris CJ, Hack W, Gray NE, Kulik V, et al. The novel estrogen receptor modulator STX attenuates Amyloid-β neurotoxicity in the 5XFAD mouse model of Alzheimer's disease. Neurobiol Dis 2022;174:105888. https://doi.org/10.1016/j.nbd.2022.105888.

[50] Paganini-Hill A, Henderson VW. Estrogen Deficiency and Risk of Alzheimer's Disease in Women. Am J Epidemiol 1994;140:256–61. https://doi.org/10.1093/oxfordjournals.aje.a117244.

[51] Cho SM, Lee S, Yang S-H, Kim HY, Lee MJ, Kim HV, et al. Age-dependent inverse correlations in CSF and plasma amyloid-β(1–42) concentrations prior to amyloid plaque

deposition in the brain of 3xTg-AD mice. Sci Rep 2016;6:20185. https://doi.org/10.1038/srep20185.

[52] Botella Lucena P, Vanherle S, Lodder C, Gutiérrez De Ravé M, Stancu I-C, Lambrichts I, et al. Blood-based Aβ42 increases in the earliest pre-pathological stage before decreasing with progressive amyloid pathology in preclinical models and human subjects: opening new avenues for prevention. Acta Neuropathol (Berl) 2022;144:489–508. https://doi.org/10.1007/s00401-022-02458-9.

[53] Ghiso J, Shayo M, Calero M, Ng D, Tomidokoro Y, Gandy S, et al. Systemic Catabolism of Alzheimer's Aβ40 and Aβ42. J Biol Chem 2004;279:45897–908. https://doi.org/10.1074/jbc.M407668200.

[54] Yu Z, Chen D, Tan C, Zeng G, He C, Wang J, et al. Physiological clearance of Aβ by spleen and splenectomy aggravates Alzheimer-type pathogenesis. Aging Cell 2022;21:e13533. https://doi.org/10.1111/acel.13533.